

---

# EXPLORATORY STATE REPRESENTATION LEARNING

---

Astrid Merckling, Nicolas Perrin-Gilbert, Alexandre Coninx, Stéphane Doncieux

ISIR, Institut des Systèmes Intelligents et de Robotique  
Sorbonne University, CNRS  
Paris, France  
astrid.merckling@isir.upmc.fr

## ABSTRACT

Not having access to compact and meaningful representations is known to significantly increase the complexity of reinforcement learning (RL). For this reason, it can be useful to perform state representation learning (SRL) before tackling RL tasks. However, obtaining a good state representation can only be done if a large diversity of transitions is observed, which can require a difficult exploration, especially if the environment is initially reward-free. To solve the problems of exploration and SRL in parallel, we propose a new approach called XSRL (eXploratory State Representation Learning). On one hand, it jointly learns compact state representations and a state transition estimator which is used to remove unexploitable information from the representations. On the other hand, it continuously trains an inverse model, and adds to the prediction error of this model a  $k$ -step learning progress bonus to form the maximization objective of a discovery policy. This results in a policy that seeks complex transitions from which the trained models can effectively learn. Our experimental results show that the approach leads to efficient exploration in challenging environments with image observations, and to state representations that significantly accelerate learning in RL tasks.

**Keywords** State Representation Learning · Pretraining · Exploration · Unsupervised Learning · Deep Reinforcement Learning.

## 1 Introduction

Recent improvements in computational power and deep learning techniques have been combined with reinforcement learning (RL) to create deep RL (DRL) algorithms capable of solving complex control tasks with continuous state and action spaces [Li, 2018]. These improvements have popularized end-to-end DRL techniques, which involve letting deep learning systems automatically learn their representations and make predictions simultaneously (i.e. without performing a feature extraction as a preliminary phase). However, despite its simplicity of design, this end-to-end strategy has three main limitations highlighted in particular by Glasmachers [2017]: (i) the sparse and delayed learning signal of temporal-difference optimization; (ii) the lack of guarantee that the roles assigned to the modules are respected (e.g. to represent image observations); (iii) the instability and slow convergence of its optimization problem.

Recently, state-of-the-art end-to-end DRL algorithms that efficiently solve these complex optimization problems face a significant computational challenge, especially in the context of continuous control tasks with visual observations [Laskin et al., 2020; Kostrikov et al., 2020]. Instead of addressing this challenge, this paper focuses on the – state representation learning (SRL) – alternative. SRL focuses on solving the state representation learning problem independently of a control task, in order to make the inputs more machine-readable for new DRL systems [Lange and Riedmiller, 2010; Jonschkowski and Brock, 2013; Böhmer et al., 2015]. This unsupervised learning strategy without reward for RL tends to circumvent the three main limitations of end-to-end DRL. This is possible by performing unsupervised state embedding pretraining from agents’ experiences which contain knowledge about themselves (proprioceptive information) and the environment properties (related to perception) common to different unknown tasks. In other words, this knowledge is task-independent information about the agent-environment, such as the agent’s configuration, the transition model of the environment (i.e. local consistency), and its structure (i.e. topology) [Morik et al., 2019].

For state representations to be good as inputs to an unseen RL task, a SRL training must observe a large diversity of transitions. Since it is often impossible to randomly explore all environment transitions, we optimize discovery policies. A standard RL policy is trained to associate an action to a state to maximize a reward. In a pure exploration context, a policy optimization can only use intrinsic rewards which estimate a degree of uncertainty about the trained models [Bubeck et al., 2009]. Our exploration strategy is one that explores the most diverse and learnable unknown transitions. However, previous strategies that also focus on such exploration belong to the context of model-based RL with planning [Shyam et al., 2019; Sekar et al., 2020], without aiming at learning an intermediate state. Instead, we propose a novel exploration strategy to learn a state embedding model, called XSRL (eXploratory State Representation Learning), which has the advantage of being computationally lighter.

XSRL consists of a twofold training procedure. In the first training procedure, XSRL learns state representations whose transitions are Markovian while advantageously reducing the image observation dimensions by filtering out unexploitable information with respect to the objective of the next observation prediction. In the second training procedure, XSRL learns discovery policies which draw actions considered as uncertain by an inverse model, and from which the state transition estimator can learn the most. Finally, in order to cope with the two sources of non-stationarity due to evolving state representations and inverse model predictions, we train two discovery policies in parallel and, given their mutual performance, reset one of them after a given number of training steps (as explained in Section 3.2.1). We use an online training with a set of agents, each half of whom follows one of the two policies.

In this article, we propose a new SRL algorithm – XSRL (eXploratory State Representation Learning) – whose main contributions can be summarized as follows. First, we introduce a novel SRL architecture which learns a state transition estimator (denoted  $\varphi$  and composed of three different modules:  $\alpha$ ,  $\beta$  and  $\gamma$ ) through the self-supervised next observation prediction objective to provide a recursive state estimation. The recursion allows the state representation to memorize information about past time steps in order to verify Markovian transitions, so as to restore full observability to environments whose real state has been replaced by image observations (Section 3.1). Second, XSRL provides a consistent exploration strategy in a rewardless environment, which is novel compared to other pure exploration strategies (Section 3.2). Third, we demonstrate the validity of XSRL representations as well as its discovery policies through quantitative and qualitative evaluations on three different environments (Section 5.1). Finally, we show improvements over other representation strategies through a comparative quantitative evaluation on unseen control tasks with a popular RL algorithm (SAC [Haarnoja et al., 2018]) (Section 5.2).

## 2 Related Work

Several other SRL algorithms with a near-future prediction objective have been proposed recently [Watter et al., 2015; Assael et al., 2015; Wahlström et al., 2015; van Hoof et al., 2016]. However, they separately learn state representations with the reconstruction objective on observations, and train a forward model on the learned states. The forward model forces the representations to retrieve information to make their transitions Markovian. The main limitation of these approaches is the inefficiency of the reconstruction objective, which forces the representations to contain unnecessary information from the observations. Because of this limitation, many empirical results in the literature show a poor generalization performance of this representation strategy to RL systems [Böhmer et al., 2015; Jaderberg et al., 2017; Shelhamer et al., 2017; de Bruin et al., 2018]. Instead, XSRL jointly learns a state transition estimator with a next observation predictor with the next observation prediction objective. On the one hand, this forces the learned state representations to retrieve information and memorize it through the recursive loop in order to restore the observability of the environment (in this work, the partial observability is due to image observations) and to verify the Markovian property. On the other hand, this forces the learned state representations to filter out unnecessary information, in particular information about distractors (i.e. elements which are not controllable or do not affect an agent).

The XSRL exploration strategy is inspired by the line of work that maximizes intrinsic rewards corresponding to prediction errors of a trained forward model, which is a form of dynamics-based curiosity [Hester and Stone, 2012; Pathak et al., 2017; Burda et al., 2018]. These strategies are often used by model-free RL algorithms such as ICM [Pathak et al., 2017], which combine intrinsic rewards with extrinsic rewards to solve the complex exploration/exploitation tradeoff. Instead, XSRL applies to rewardless environments in the SRL context, i.e. it focuses only on the complex non-stationary training of state representation models. In addition, XSRL differs in two other ways: (i) while ICM is applied to discrete actions, XSRL is applied to continuous actions, (ii) while ICM uses prediction errors of a trained forward model, XSRL uses those of an inverse model because they only depend on the controllability properties (see Eq. 3.2.2).

While the previous prediction errors of an inverse model give an uncertainty estimation of actions with respect to their controllability,  $k$ -step learning progress bonuses of the transition model ( $\varphi$ ) give an uncertainty estimation of actions with respect to their learnability. Learning progress estimation was initially proposed in the field of developmental

robotics [Oudeyer et al., 2007]. Lopes et al. [2012] initiated the estimation of learning progress bonuses to solve the exploitation/exploration tradeoff in the model-based RL domain with finite MDPs. Achiam and Sastry [2017] have scaled this approach to continuous MDPs, however it remains limited to compact observations of several dozen dimensions. We now scale the work of Achiam and Sastry [2017] to image observations and in the SRL context. Thus, XSRL trains discovery policies to also maximize  $k$ -step learning progress bonuses of  $\varphi$  to favor learnable unknown transitions. This way, the XSRL exploration strategy exploits learnable unknown transitions with a high controllability diversity criterion.

### 3 Proposed Method: XSRL

#### 3.1 State Transition Estimator

The goal of SRL is to transform high-dimensional observations into machine-readable compact representations which retrieve information about an agent and the environment and disentangle their degrees of freedom [Lesort et al., 2018]. To do this, we make the assumption with XSRL that a good state representation must contain the information needed to predict the next observation from the previous time step.

Our state transition estimator  $\varphi$  consists of two neural network parts ( $\alpha$ ,  $\beta$ ), and a common network head  $\gamma$ . While  $\alpha$  is a convolutional neural network (CNN) to process image observations,  $\beta$  is a multilayer perceptron (MLP) to process the concatenated action and state vectors. Finally, the common network head  $\gamma$  is a MLP to process the concatenated output vectors of the two first network parts to estimate next state vectors ( $\mathbf{s}_{t+1}$ ).

According to the graph in Fig. 1(a), from current observation  $\mathbf{o}_t$ , action  $\mathbf{a}_t$  and state  $\mathbf{s}_t$ , information is compactly merged into a next state  $\mathbf{s}_{t+1}$  through the intermediate functions ( $\alpha$ ,  $\beta$ ,  $\gamma$ ). Because of the recursive loop on the state representation,  $\varphi$  bootstraps from an initial state drawn from a Gaussian distribution of mean zero and standard deviation 0.02. Putting all the functions together, we get the following definition of  $\varphi$  predictions:

$$\begin{aligned}\mathbf{s}_{t+1} &= \gamma([\alpha(\mathbf{o}_t), \beta([\mathbf{s}_t, \mathbf{a}_t])]) \\ \mathbf{s}_{t+1} &= \varphi([\mathbf{o}_t, \mathbf{s}_t, \mathbf{a}_t])\end{aligned}\tag{1}$$

where we abbreviate the state transition estimator network ( $\alpha$ ,  $\beta$ ,  $\gamma$ ) by  $\varphi$  and their parameters are concatenated into the following parameter set  $\theta_\varphi = \{\theta_\alpha, \theta_\beta, \theta_\gamma\}$ . The implementation details of the whole neural network are displayed in Table 3.

$\varphi$  is trained jointly with a next observation predictor  $\omega$  thanks to the next observation prediction objective.  $\omega$  is a CNN with transposed convolution layers<sup>1</sup> to deterministically predict from the outputs of  $\varphi$  (i.e.  $\mathbf{s}_{t+1}$ ) the next observations as follows  $\omega(\mathbf{s}_{t+1}) = \hat{\mathbf{o}}_{t+1}$ . This yields the following prediction error:

$$\|\hat{\mathbf{o}}_{t+1} - \mathbf{o}_{t+1}\|_2^2\tag{2}$$

All the parameters of  $\omega$  are gathered in a single parameter set  $\theta_\omega$ . The corresponding training process will be described with the complete XSRL training process in Section 3.3.

Thanks to this joint training of  $\varphi$  and  $\omega$ , XSRL builds compact state representations which contain the information needed to predict the next observations, which is deterministic and simple enough to be modeled. In the context where the robot's state space follows Markovian transitions but is unknown and only image observations are available, the environment becomes partially observable, which may be due to perceptual aliasing or dynamic transitions. We therefore force  $\varphi$  to memorize in the state representations (through the recursive loop) the information of past time steps in order to restore the Markovian property of the learned state transitions.

Indeed, to predict the next observation with  $\omega$ , the next state representation  $\mathbf{s}_{t+1} = \varphi([\mathbf{o}_t, \mathbf{s}_t, \mathbf{a}_t])$  must contain the information of past and current time steps. As this information cannot only be retrieved from  $\mathbf{o}_t$  and  $\mathbf{a}_t$ , some of it must be memorized in  $\mathbf{s}_t$  through the state recursive loop. In this way, the state representations learned by XSRL form Markovian transitions that translate mathematically as follows:

$$P(\mathbf{s}_{t+1}|\mathbf{s}_t, \mathbf{a}_t) = P(\mathbf{s}_{t+1}|\mathbf{s}_t, \mathbf{a}_t, \mathbf{s}_{t-1}, \mathbf{a}_{t-1}, \dots, \mathbf{s}_0, \mathbf{a}_0)\tag{3}$$

for all states  $\mathbf{s}_{t+1}, \mathbf{s}_t \in \mathcal{S} \subset \mathbb{R}^{S_d}$  and actions  $\mathbf{a}_t \in \mathcal{A} \subset \mathbb{R}^{A_d}$ . In particular, this forces state representations to verify the local consistency and often the topology (or connectivity) of the environment, since otherwise they would not be able to restore the observability [Morik et al., 2019].

The local consistency of an environment is related to the transition model, i.e. the way an agent transitions from one state to another, but without the reward information. In order for the state representations to verify this property in

<sup>1</sup>We used the 2D transposed convolution operator provided by PyTorch.

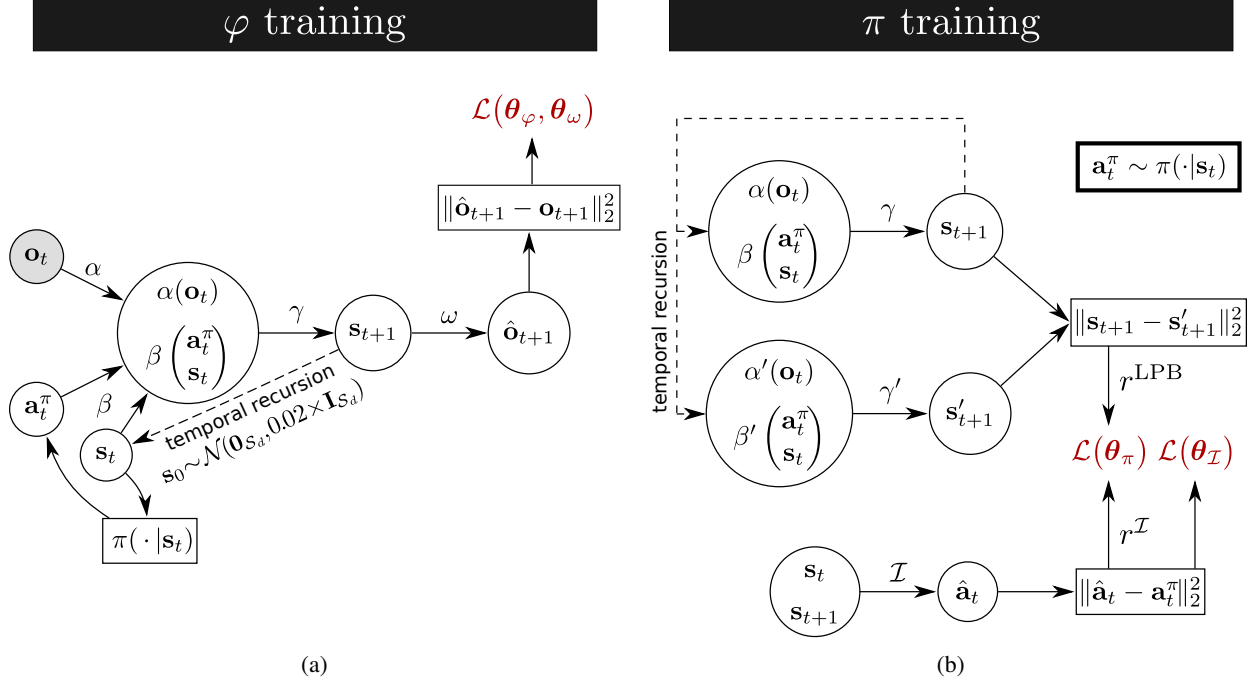


Figure 1: **(a)** XSRL learning process of state representations by jointly training a state transition estimator  $\varphi$  formed by  $(\alpha, \beta, \gamma)$  and a head  $\omega$  with the next observation prediction objective, where actions are sampled from one of the two discovery policies  $\pi_1$  and  $\pi_2$  (each policy is used on half of the agents in an online manner, as explained in Section 3.3). **(b)** XSRL learning process of a discovery policy by minimizing  $\mathcal{L}(\theta_\pi)$  which is related to the intrinsic rewards (for clarity reasons,  $\pi$  represents either  $\pi_1$  or  $\pi_2$ ). Intrinsic rewards are formed of two main terms. (i)  $r^{\mathcal{I}}$ : prediction errors of an inverse model  $\mathcal{I}$  (also used in  $\mathcal{L}(\theta_{\mathcal{I}})$ ); (ii)  $r^{\text{LPB}}$ :  $k$ -step learning progress bonuses of  $\varphi$  where the parameters of  $\varphi'$  formed by  $(\alpha', \beta', \gamma')$  are delayed by  $k$  training steps and kept fixed.

environments with acceleration, it is necessary for them to be linked to the environment dynamics. For example, a state representation of a torque-controlled robot requires to verify this property to retrieve his velocities and positions, which are necessary to predict the next observation.

Alternatively, the topology of an environment corresponds to its structure, i.e. properties independent of an agent. For example, a state representation of a navigator robot (like the one in TurtleBot Maze) requires to verify in addition to the local consistency this property to retrieve his orientation and position. Indeed, to localize an agent with perceptual aliasing, the state representation must memorize the environment structure independently of the agent and so invariant with respect to his orientation and position as noticed previously by Böhmer et al. [2013].

Another advantage of XSRL state representations is that they remove unnecessary information for predicting next observations so as to preserve useful information to predict the change produced by an action in the next observation. This has two main merits: (i) XSRL can effectively cope with dimensionality reduction, (ii) aleatoric uncertainty such as random noise or other random distractors will be removed by state representations, which is key to the success of XSRL pure exploration strategy. As shown by Burda et al. [2018], policies learned with a dynamics-based curiosity tend to be attracted by aleatoric uncertainty related to the environment transitions. Our results in Section 5.1 will show that XSRL trained discovery policies are not attracted to such transitions in TurtleBot Maze environment where one of the walls has a randomly sampled color at each time step.

## 3.2 Discovery in the Face of Uncertainty

### 3.2.1 Over-Commitment

A problem that arises in pure exploration with dynamics-based curiosity is the non-stationarity of intrinsic rewards. Specifically, as in other dynamics-based curiosity explorations from image observations, two sources of non-stationarity emerge [Burda et al., 2018]: (i) the model trained concurrently with discovery policies improves during training and its prediction errors minimize on visited transitions, (ii) the state representations evolve during  $\varphi$  training. Such a

non-stationary training signal tends to attract policies in poor local optima. Indeed, when transitions maximizing intrinsic rewards are sufficiently visited, they become known and the policy generally cannot escape from this solution stuck in a poor local optima. Shyam et al. [2019] have popularized this problem as “over-commitment”. The latter proposed to circumvent it by training from scratch a new policy. This is what we propose to do with XSRL by training two discovery policies in parallel called  $\pi_1$  and  $\pi_2$ , and every  $T_{\text{reset}}$  iterations reset the policy with the lowest cumulative intrinsic rewards without the entropy term.

### 3.2.2 Intrinsic Rewards

The intrinsic rewards to be maximized by XSRL discovery policies are a combination of the following terms: (i) prediction errors of an inverse model which should be maximized on transitions which are complex with respect to their controllability, (ii)  $k$ -step learning progress bonuses of the state transition estimator ( $\varphi$ ) which should be maximized on transitions with high learnability with respect to the next observation prediction, (iii) a policy entropy estimation to ensure convergence stability. Fig. 1(b) shows the graph corresponding to the calculation of the two main terms (i) and (ii).

**Inverse model** While previous dynamics-based curiosity methods [Pathak et al., 2017; Burda et al., 2018] typically use a forward model to indirectly estimate an action uncertainty, we use an inverse model. Pathak et al. [2017] train an inverse model to learn state representations (without the goal to transfer them to new learning tasks). Prediction errors of a forward model on such representations would depend only on the elements controllable by an agent. Instead, we train a state transition model with a next observation predictor to learn state representations (with the goal to transfer them to new learning tasks). Prediction errors of a forward model on such representations would depend on what affect the camera due to the next observation prediction objective. For example, large variations in pose or illumination would be considered difficult to predict. Thus, maximizing prediction errors of a forward model from XSRL learned representations would favor actions that cause large observation changes which are not useful to discover the environment. Alternatively, prediction errors of an inverse model are only related to the difficulty of the state transitions. In summary, with XSRL learned representations, while prediction errors of a forward model depend on visibility properties, those of an inverse model depend on controllability properties. It is this controllability diversity criterion that motivated us to train an inverse model to indirectly estimate an action uncertainty.

An inverse model, takes as input a pair of consecutive states ( $s_t, s_{t+1}$ ) to predict the action  $\hat{a}_t = \mathcal{I}(s_{t+1}, s_t)$  executed by an agent to obtain the next state  $s_{t+1}$ . The prediction errors to be maximized by the discovery policies and minimized by the inverse model are calculated as follows:

$$r^{\mathcal{I}}(\hat{a}_t, \mathbf{a}_t^\pi) = \|\hat{a}_t - \mathbf{a}_t^\pi\|_2^2 \quad (4)$$

where the action  $\mathbf{a}_t^\pi$  is sampled from  $\pi_1$  and  $\pi_2$  equally because half of the set of agents is associated with one of them. The training process of an inverse model is detailed later in Section 3.3.

**Learning progress bonuses** To ensure that actions considered uncertain by the inverse model (given the state representations learned by  $\varphi$ ) lead to learnable unknown transitions, we use  $k$ -step learning progress bonuses of  $\varphi$ . This is a way to approximate the amplitude change in the parameter space produced by  $k$  training steps [Achiam and Sastry, 2017]. The larger this measure is on a new transition, the more  $\varphi$  and  $\omega$  can reduce the prediction error of the corresponding next observation and thus generalize better. Maximizing these bonuses allows, during XSRL training, to progressively increase the complexity of the observed transitions, thus ensuring that some unknown transitions, too complex to be learned with the current  $\varphi$  solution, are not favored until other easier transitions are observed. In other words, it ensures that the difficulty of transitions with respect to controllability intersects with their learnability by  $\varphi$ . Furthermore, once the inverse model has converged, these bonuses will complete the convergence of  $\varphi$  by increasing the diversity of transitions with respect to the next observation prediction objective. For example, if at new transitions there is deterministically predictable information, these bonuses allow visiting them to further improve the generalization performance of the model  $\varphi$ .

We adapted the  $k$ -step learning progress bonus proposed by Achiam and Sastry [2017] into the deterministic setting of our state transition model  $\varphi$ . To do so, we introduce  $\varphi'$  formed by  $(\alpha', \beta', \gamma')$  with parameters delayed by  $k$  iterations and kept frozen. The  $k$ -step learning progress bonuses of  $\varphi$  to be maximized by the two discovery policies result in:

$$r^{\text{LPB}}(\mathbf{o}_t, s_t, \mathbf{a}_t^\pi) = \|\varphi([\mathbf{o}_t, s_t, \mathbf{a}_t^\pi]) - \varphi'([\mathbf{o}_t, s_t, \mathbf{a}_t^\pi])\|_2^2 \quad (5)$$

where the action  $\mathbf{a}_t^\pi$  is sampled from the discovery policy  $\pi_1$  or  $\pi_2$  that an agent follows.

**Policy entropy estimation** For better convergence stability, discovery policies must maximize in addition to intrinsic rewards their entropy estimation. Following Haarnoja et al. [2018], we use an automatic weight tuning of this term  $w_{\mathcal{H}}$



(a.k.a. temperature). This technique uses an optimization algorithm of the training type to automatically adjust this hyperparameter with respect to the difference between the estimated entropy and a target value  $\bar{\mathcal{H}}$  to match as follows:

$$w_{\mathcal{H}} [\mathcal{H}(\pi(\cdot|\mathbf{s}_t)) - \bar{\mathcal{H}}] \quad (6)$$

As in the original implementation of the automatic tuning of the entropy term weight, the target entropy to match  $\bar{\mathcal{H}}$  is equal to minus the action dimension  $-\mathcal{A}_d$ , see [Haarnoja et al., 2018] for more details.

### 3.2.3 Discovery Policies

Now that we have detailed the three terms for computing intrinsic rewards, we explain how we train discovery policies to maximize them. In this work, we study environments with continuous action spaces. The general approach to learn a policy in this case is to model it as a multivariate Gaussian distribution with a diagonal covariance matrix from states to actions [Haarnoja et al., 2018]. To do this, we use a neural network with a first common part, then one head  $\mu_{\pi}$  with parameters  $\theta_{\mu}$  to predict a mean vector, and a second head  $\Sigma_{\pi}$  with parameters  $\theta_{\Sigma}$  to predict the diagonal covariance elements of a covariance matrix. The outputs of these two heads, which have the same dimensions as the action space, allow us to parameterize a policy, so that it follows a Gaussian distribution defined as:

$$\pi(\cdot|\mathbf{s}_t) \triangleq \mathcal{N}(\mu_{\pi}(\mathbf{s}_t), \Sigma_{\pi}(\mathbf{s}_t)) \quad (7)$$

All parameters of a discovery policy  $\pi$  are gathered in a single parameter set  $\theta_{\pi} = \{\theta_{\mu}, \theta_{\Sigma}\}$ . The reparametrization trick [Kingma and Welling, 2014] is used to sample an action from a policy (i.e.  $\mathbf{a}_t^{\pi} \sim \pi(\cdot|\mathbf{s}_t)$ ) to keep all its parameters differentiable:

$$\mathbf{a}_t^{\pi} \triangleq \mu_{\pi}(\mathbf{s}_t) + \epsilon_t \times \Sigma_{\pi}(\mathbf{s}_t) \quad , \quad \epsilon_t \sim \mathcal{N}(\mathbf{0}_{\mathcal{A}_d}, \mathbf{I}_{\mathcal{A}_d}) \quad (8)$$

The two discovery policies ( $\pi_1$  and  $\pi_2$ ) can be optimized directly from the intrinsic reward gradients. Indeed, intrinsic rewards are computed with prediction errors of an inverse model,  $k$ -step learning progress bonuses of  $\varphi$ , and a policy entropy estimation, all of which use actions sampled from  $\pi_1$  or  $\pi_2$ . Thus, intrinsic reward gradients can be used to train discovery policies in a supervised learning manner, as was done previously by Pathak et al. [2019]. Thus, our discovery policy training strategy is based on minimizing the following loss function:

$$- (w_{\mathcal{I}} r^{\mathcal{I}}(\hat{\mathbf{a}}_t, \mathbf{a}_t^{\pi}) + w_{\text{LPB}} r^{\text{LPB}}(\mathbf{o}_t, \mathbf{s}_t, \mathbf{a}_t^{\pi}) + w_{\mathcal{H}} \mathcal{H}(\pi(\cdot|\mathbf{s}_t))) \quad (9)$$

Minimizing this loss function, which amounts to maximize the intrinsic rewards, allows a training type of optimization. The corresponding training process is described in the next section.

The fact that we minimize a deterministic loss does not mean that there is no probabilistic interpretation. Indeed as explained previously, sources of prediction errors of an inverse model may be related to action uncertainty dependent on the controllability of learned state transitions;  $k$ -step learning progress bonuses of  $\varphi$  may be related to action uncertainty dependent on the learnability of state transitions. Furthermore, the estimated entropy of a policy is related to action uncertainty with respect to learned state representations. Thus, our two discovery policies learn a probability over the action space that tends to sample actions which maximize these uncertainties.

## 3.3 Optimization Process

Let us define the notations for the training examples we manipulate in our online training procedure. There is an even number  $B \geq 2$  of agents in parallel, where  $b \in \llbracket 1, B \rrbracket$ , and each of them is initialized in the same fixed configuration so that an effective exploration is required to visit the most diverse transitions of the environment. At time step  $t$ , a training example for  $(\varphi, \omega)$  is an element of the form  $(\mathbf{o}_{t+1}^{(b)}, \mathbf{o}_t^{(b)}, \mathbf{s}_t^{(b)}, \mathbf{a}_t^{\pi(b)})$ , composed respectively of the next observation and current observation, a state representation estimated at previous time step (i.e.  $t - 1$ ), and an action sampled from one of the two discovery policies as  $\mathbf{a}_t^{\pi(b)} \sim \pi(\cdot|\mathbf{s}_t^{(b)})$  (following the sampling process defined in Eq. 8). Specifically, each half of the set of  $B$  agents follows one of the two policies ( $\pi_1$  and  $\pi_2$ ). A state transition estimator  $\varphi$  composed of three modules  $(\alpha, \beta, \gamma)$  estimates from the triplet input  $(\mathbf{o}_t^{(b)}, \mathbf{s}_t^{(b)}, \mathbf{a}_t^{\pi(b)})$  the next state  $\mathbf{s}_{t+1}^{(b)}$ , from which  $\omega$  predicts the next observation  $\hat{\mathbf{o}}_{t+1}^{(b)}$ .

The optimization problem to simultaneously train  $\varphi$  and  $\omega$ , is the minimization of the following objective function (based on the next observation prediction error of Eq. 1):

$$\mathcal{L}(\theta_{\varphi}, \theta_{\omega}) = \frac{1}{B} \sum_{b=1}^B \|\omega(\mathbf{s}_{t+1}^{(b)}) - \mathbf{o}_{t+1}^{(b)}\|_2^2 \quad (10)$$

After each  $b$ -agent has executed the action  $\mathbf{a}_t^{\pi(b)}$ , the backpropagation computes the partial derivatives of this objective function with respect to the parameter sets  $\theta_{\varphi}$  and  $\theta_{\omega}$  in order to perform a training step.

### 3.3.1 Different Update Interval

The inverse model and the two discovery policies are trained in parallel to the above training. Instead of performing a training step after every agent performs an action, it is performed after a chosen update interval ( $T_\pi$ ). Since the policy optimization is much more sensible to the i.i.d. hypothesis, we use the largest possible sampling period  $k$  for these two types of optimization ( $k$  also corresponds to the number of training steps whose the parameters of  $\varphi'$  are delayed). To do this, we specify an update interval  $T_\pi \in \mathbb{Z}^+$  which is the number of time steps before a training step is performed on the parameters of the inverse model and the parameters of the two discovery policies. Then, given a chosen batch size  $B_\pi \in \mathbb{Z}^+$  and the number  $B$  of agents running in parallel, a batch of training examples is formed of  $\lfloor \frac{B_\pi}{B} \rfloor$  samplings. Then, to maximize the independence between each of these samplings, we define a sampling period to be  $k = \lfloor \frac{T_\pi B}{B_\pi} \rfloor$ .

The optimization problem to train the inverse model is the minimization of the following objective function (based on the action prediction error of Eq. 4):

$$\mathcal{L}(\theta_{\mathcal{I}}) = \frac{1}{B_\pi} \sum_{i=0}^{\lfloor \frac{B_\pi}{B} \rfloor - 1} \sum_{b=1}^B \left\| \mathcal{I}(\mathbf{s}_{t+1-k}^{(b)}, \mathbf{s}_{t-k}^{(b)}) - \mathbf{a}_{t-k}^{\pi_{(b)}} \right\|_2^2 \quad (11)$$

The backpropagation computes the partial derivatives of this objective function with respect only to the parameter set  $\theta_{\mathcal{I}}$ .

The optimization problem to train the two discovery policies is the minimization of the following objective function (based on the loss of Eq. 9):

$$\mathcal{L}(\theta_\pi) = \frac{1}{B_\pi} \sum_{i=0}^{\lfloor \frac{B_\pi}{B} \rfloor - 1} \sum_{b=1}^B - \left[ w_{\mathcal{I}} r^{\mathcal{I}}(\hat{\mathbf{a}}_{t-k}^{\pi_{(b)}}, \mathbf{a}_{t-k}^{\pi_{(b)}}) + w_{\text{LPB}} r^{\text{LPB}}(\mathbf{o}_{t-k}^{(b)}, \mathbf{s}_{t-k}^{(b)}, \mathbf{a}_{t-k}^{\pi_{(b)}}) - w_{\mathcal{H}} \log(\mathbf{a}_{t-k}^{\pi_{(b)}}) \right] \quad (12)$$

where the parameter set  $\theta_{\mathcal{I}}$  is frozen, and that of  $\varphi'$  is updated every  $k$  iterations with that of  $\varphi$  and kept frozen. More specifically, the backpropagation computes the partial derivatives of this objective function with respect to the parameter set of one of the two discovery policies (i.e.  $\theta_{\pi_1}$  or  $\theta_{\pi_2}$ ). This objective function is low where the inverse model fails to predict actions, and learning progress bonuses are large.

Finally, to automatically tune the temperature  $w_{\mathcal{H}}$ , we minimize the following objective function:

$$\mathcal{L}(w_{\mathcal{H}}) = \frac{1}{B_\pi} \sum_{i=0}^{\lfloor \frac{B_\pi}{B} \rfloor - 1} \sum_{b=1}^B w_{\mathcal{H}} \left[ -\log(\mathbf{a}_{t-k}^{\pi_{(b)}}) - \bar{\mathcal{H}} \right] \quad (13)$$

As explained in Section 3.2.1, we choose to simultaneously train two discovery policies to mitigate the “over-commitment” [Shyam et al., 2019]. Specifically, our XSRL algorithm (as displayed in Algo. 1) resets the policy with the lowest intrinsic rewards without the entropy term as follows:  $w_{\mathcal{I}} r^{\mathcal{I}}(\hat{\mathbf{a}}_{t-k}^{\pi_{(b)}}, \mathbf{a}_{t-k}^{\pi_{(b)}}) + w_{\text{LPB}} r^{\text{LPB}}(\mathbf{o}_{t-k}^{(b)}, \mathbf{s}_{t-k}^{(b)}, \mathbf{a}_{t-k}^{\pi_{(b)}})$  accumulated over  $T_{\text{reset}}$  time steps (defined in Table 3). It is also a way to re-explore already learned transitions by performing suboptimal actions. Indeed, a policy trained from scratch must go through all types of transitions again. This ensures a better diversity of transitions visited throughout the XSRL training procedure and thus mitigates the overfitting peculiar to deep neural networks.

In summary, our XSRL algorithm described in Algo. 1, performs four types of optimization: (i) of a state transition estimator with Eq. 10, (ii) of an inverse model with Eq. 11, (iii) of two distinct discovery policies with Eq. 12, (iv) of an automatic temperature tuning with Eq. 13. This XSRL training procedure is repeated until the convergence of the parameters updated with the next observation prediction objective (i.e.  $\theta_\varphi$  and  $\theta_\omega$ ). See Table 3 for more details on the hyperparameters of our XSRL implementation.

Fig. 2 shows the two phases of XSRL considered in this work. (a): the twofold training procedure that XSRL follows in order to provide good state representations to solve unseen control tasks. (b): shows the deployment of such a solution  $\varphi$  to predict state representations for an unseen RL task. In particular, we no longer use discovery policies, an inverse model, and a  $k$ -step delayed model  $\varphi'$ , all corresponding to the exploration strategy of XSRL. We also discard the network head  $\omega$  related to the self-supervised next observation prediction objective.

## 4 Experimental Setup

This section describes a systematic evaluation of all criteria that our XSRL algorithm must verify. XSRL must learn state representations which (i) retrieve information (possibly by memorizing through past time steps) to guarantee that

**Algorithm 1** XSRL algorithm

- 
- 1: **Initialization:** Prepare an even number  $B \geq 2$  of agents, reset to the same fixed starting state in an instance of the same environment  $\mathbf{env}^{(b)}$ , the first  $\frac{B}{2}$  agents will be associated with  $\pi_1$ , and the other  $\frac{B}{2}$  agents will be associated with  $\pi_2$ . Choose for the inverse model and discovery policies an update interval  $T_\pi \in \mathbb{Z}^+$ , a batch size  $B_\pi \in \mathbb{Z}^+$  and compute the sampling period as  $k = \lfloor \frac{T_\pi B}{B_\pi} \rfloor$ ; choose the reset interval  $T_{\text{reset}}$ ; choose intrinsic reward weight terms:  $w_{\mathcal{I}}, w_{\text{LPB}}$ ; choose the entropy target  $\mathcal{H}$  for the automatic tuning of the temperature (i.e.  $w_{\mathcal{H}}$ ).  
 At each reset of a  $b$ -th agent: randomly initialize the state  $\mathbf{s}_0^{(b)}$  from a Gaussian distribution of mean zero and standard deviation 0.02.  
 Randomly initialize: a state representation transition network  $\varphi$  formed by  $(\alpha, \beta, \gamma)$  following the architecture described in Fig. 1A with parameters  $\theta_\varphi = \{\theta_\alpha, \theta_\beta, \theta_\gamma\}$  and use these parameters to initialize  $\varphi'$  formed by  $(\alpha', \beta', \gamma')$ ; a next observation predictor network  $\omega$  with parameters  $\theta_\omega$ ; an inverse model  $\mathcal{I}$  with parameters  $\theta_{\mathcal{I}}$ ; two distinct discovery policies  $\pi_1$  and  $\pi_2$  with parameters  $\theta_{\pi_1}$  and  $\theta_{\pi_2}$  respectively.
  - 2: **Output:** A task-independent state transition estimator  $\varphi$  formed of three modules  $(\alpha, \beta, \gamma)$  to predict compact state representations.
  - 3: **while**  $(\theta_\varphi, \theta_\omega)$  have not converged **do**
  - 4:   Sample actions from each of the discovery policies ( $\pi_1$  and  $\pi_2$ ) on half of the  $B$  agents as:
 
$$\mathbf{a}_t^{\pi^{(b)}} = \mu_\pi(\mathbf{s}_t^{(b)}) + \epsilon_t^{(b)} \times \Sigma_\pi(\mathbf{s}_t^{(b)}) \quad , \quad \epsilon_t^{(b)} \sim \mathcal{N}(\mathbf{0}_{A_d}, \mathbf{I}_{A_d})$$
  - 5:   Perform the action with every agent:  $\mathbf{o}_{t+1}^{(b)} \leftarrow \mathbf{env}^{(b)}(\mathbf{a}_t^{\pi^{(b)}})$
  - 6:   Predict next state representations for all  $B$  agents:
 
$$\mathbf{s}_{t+1}^{(b)} = \gamma \left( \left[ \alpha(\mathbf{o}_t^{(b)}), \beta \left( [\mathbf{s}_t^{(b)}, \mathbf{a}_t^{\pi^{(b)}}] \right) \right] \right)$$
  - 7:   Compute  $\mathcal{L}(\theta_\varphi, \theta_\omega)$  from Eq. 10.
  - 8:   Perform a training step on  $\mathcal{L}(\theta_\varphi, \theta_\omega)$  w.r.t.  $\theta_\varphi$  and  $\theta_\omega$ .
  - 9:   **every**  $T_\pi$  **iterations do**  
     Compute  $\mathcal{L}(\theta_{\mathcal{I}})$  with Eq. 11 and perform a training step w.r.t.  $\theta_{\mathcal{I}}$ .  
     Compute  $\mathcal{L}(\theta_{\pi_1})$  with Eq. 12 and perform a training step w.r.t.  $\theta_{\pi_1}$ .  
     Compute  $\mathcal{L}(\theta_{\pi_2})$  with Eq. 12 and perform a training step w.r.t.  $\theta_{\pi_2}$ .  
     Compute  $\mathcal{L}(w_{\mathcal{H}})$  with Eq. 13 and perform a training step w.r.t.  $w_{\mathcal{H}}$ .  
     Update the parameters of  $\varphi'$  with those of  $\varphi$  and keep them frozen.
  - 10:   **every**  $T_{\text{reset}}$  **iterations do**  
     Reset one of the two discovery policies with the lowest intrinsic reward without the entropy term (i.e.  $w_{\mathcal{I}} r^{\mathcal{I}}(\hat{\mathbf{a}}_{t-k_i}^{\pi^{(b)}}, \mathbf{a}_{t-k_i}^{\pi^{(b)}}) + w_{\text{LPB}} r^{\text{LPB}}(\mathbf{o}_{t-k_i}^{(b)}, \mathbf{s}_{t-k_i}^{(b)}, \mathbf{a}_{t-k_i}^{\pi^{(b)}})$ ) accumulated over  $T_{\text{reset}}$  time steps.
  - 11: **end while**
- 

their transitions are Markovian, (ii) filter unnecessary information. Furthermore, XSRL must learn discovery policies which (iii) guide agents quickly through most diverse transitions while avoiding unlearnable ones. Finally, after XSRL pretraining, the state transition estimator  $\varphi$  must (iv) provide advantageous inputs to solve unseen control tasks.

We evaluate the criterion (i) with the average of the next observation prediction errors on a training dataset and a test dataset. While the former is formed from samples generated during the training process, the latter is carefully designed for each environment, as described in Section 4.2.6. The lower this error measure is, the more the state transitions verify the Markovian property, because the next observation prediction depends only on the previous time step (as explained in Section 3.1). Furthermore, we measure the quantitative performance obtained by RAE (Regularized Autoencoder [Ghosh et al., 2019]) with the average of observation reconstruction errors to give a quantitative comparison with a state-of-the-art algorithm. However, since it is more complicated to predict the next observation than to reconstruct it, it is expected that the latter will perform better.

We evaluate the criterion (ii) of state representations and the criterion (iii) of discovery policies by training XSRL in our TurtleBot Maze environment by injecting aleatoric uncertainty into its transitions. To do this, we randomly sample at every time step a color for the small vertical wall in the lower branch of the maze, just in front of the initial state location of the robot, as shown in the top row of Fig. 5. We obtain a quantitative evaluation of our results with the same error measure as before, while also qualitatively evaluating our results by observing that XSRL does not attempt to predict the random wall color.

In addition to verify the criterion (iii), we perform other exploration evaluations during the state embedding pretraining of XSRL. First qualitatively by visualizing the coverage performance of XSRL discovery policies, then quantitatively



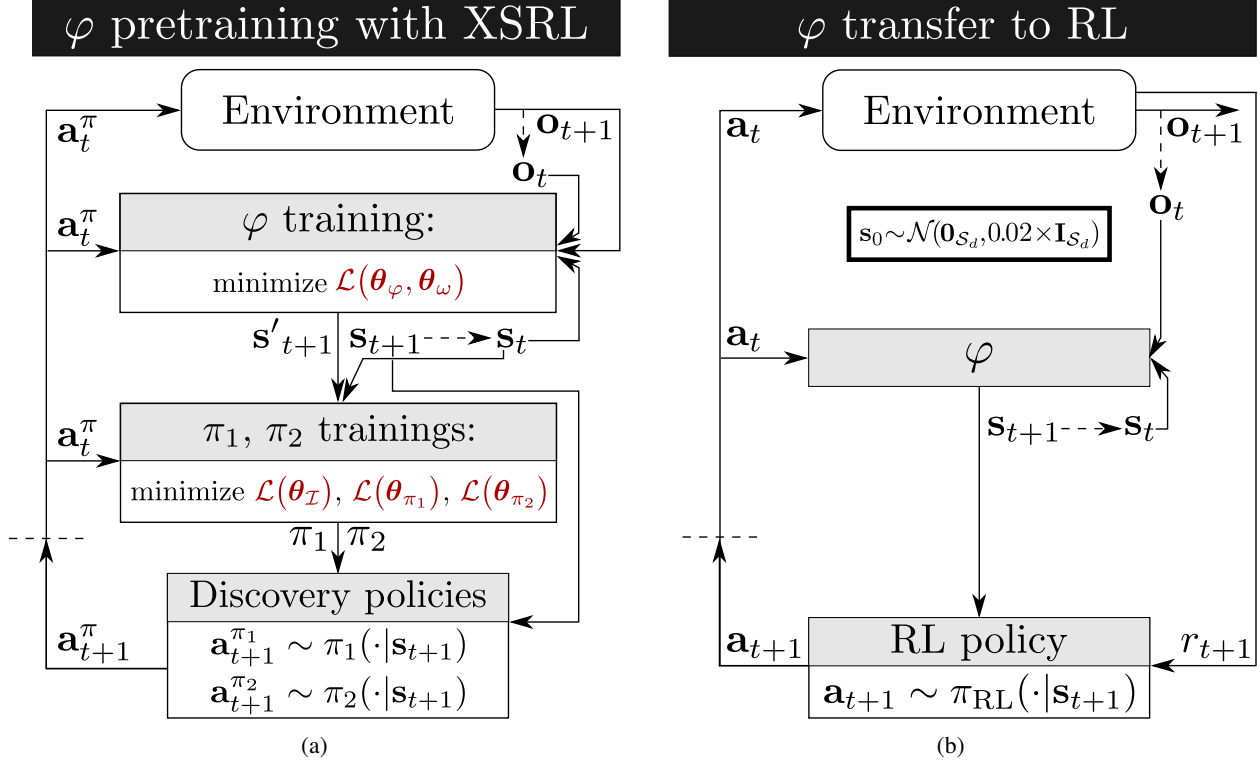


Figure 2: **(a)** Schematic representation of the XSRL twofold training procedure to provide compact state representations by jointly training a state transition estimator  $\varphi$  with a next observation predictor  $\omega$ , guided by two discovery policies  $\pi_1$  and  $\pi_2$  (for clarity reasons, in the exponents of sampled actions  $\pi$  represents either  $\pi_1$  or  $\pi_2$ ) in an online manner with several agents in parallel (the first half of the agents following  $\pi_1$  and the other  $\pi_2$ ). Here  $\mathbf{s}_{t+1} = \varphi([\mathbf{o}_t, \mathbf{s}_t, \mathbf{a}_t])$ , and  $\mathbf{s}'_{t+1} = \varphi'([\mathbf{o}_t, \mathbf{s}_t, \mathbf{a}_t])$  where  $\varphi'$  is the same network of  $\varphi$  whose parameters are delayed by  $k$  iterations and kept frozen. **(b)** A schematic illustration of the transfer of the pretrained state representation model ( $\varphi$ ) to an unknown RL task.

by counting the average number of training steps before one of the 32 agents reaches the other end of the maze. Furthermore, since  $\|\mathbf{o}_{t+1} - \hat{\mathbf{o}}_{t+1}\|_2^2$  is a useful prediction error measure to quantitatively evaluate the generalization performance of  $\omega$  which is directly related to the performance of discovery policies, a high error measure will indicate that the XSRL exploration strategy is not efficient enough. To complete the evaluation of the discovery policy criterion, we also compare with two XSRL ablations:

- XSRL-MaxEnt: trains a policy to maximize its entropy estimation;
- XSRL-random: uses a random policy which samples actions uniformly from the action space.

Here, XSRL-random is expected to give minimal performance, while XSRL-MaxEnt should be worse than XSRL, as it only depends on the policy distribution.

We evaluate the criterion (iv) with the transfer of XSRL  $\varphi$  solution to unseen RL tasks. During RL training, the environment provides an agent with extrinsic rewards to train an optimal policy, while  $\varphi$  provides compact observations as shown in Fig. 2(b). To rigorously conduct this evaluation, we use a popular RL algorithm with continuous actions – SAC (Soft Actor-Critic) [Haarnoja et al., 2018] – on each of the tasks in the three environments shown in Fig. 3. These continuous control tasks (presented in detail in Section 4.2), are challenging because of their high-dimensional observation spaces consisting of a camera. In order to obtain a quantitative evaluation of our results, we compare the performance between other representation strategies detailed below.

#### 4.1 Baselines

We compare the performances of XSRL representations on unseen RL tasks to the following five baselines: ground truth, open-loop, position, RAE, random network.

Of all these baselines, only RAE (Regularized Autoencoder [Ghosh et al., 2019]) is a state-of-the-art SRL method. We train it using the same three rewardless environments with fixed state initializations as for XSRL described in Section 4.2.4. However, since it has no associated exploration strategy to generate observations, we use either a random policy as previously done by Yarats et al. [2019], or an effective exploration (indicated by the suffix *-explor*). In TurtleBot Maze, this effective exploration corresponds to a random policy with 50 time steps and random initialization, while in the two torque-controlled environments, it has 0.5 probability to take a random action and otherwise to take an action sampled from an optimal policy pretrained in the RL context (i.e. where extrinsic rewards are available) with SAC from the ground truth representations.

RAE is a deterministic alternative to the variational autoencoder (VAE) [Kingma and Welling, 2014], which preserves the regularizing effect of the latter. To the best of our knowledge, we do not know of any other method than RAE, belonging to the SRL context, that achieves state-of-the-art performance on the torque-controlled tasks of the DeepMind Control Suite (DMControl) benchmark [Tassa et al., 2018] with visual observations considered in this work. Specifically, on the DMControl benchmark, Yarats et al. [2019] obtain results where RAE performs as well as PlaNet [Hafner et al., 2018] with the SAC algorithm [Haarnoja et al., 2018].

We also use a random network representation where, instead of training a network, its parameters are simply fixed to random values sampled from a Gaussian distribution of mean zero and standard deviation 0.02. This strategy without any training was popularized for classification tasks by Jarrett et al. [2009] and then for RL task by Gaier and Ha [2019].

We use only in the InvertedPendulum environment, the position baseline which corresponds to position measurements without velocities. The absence of velocities allows us to show the relevance of such dynamic information to solve the swing up task. Comparison with its performance would show that XSRL extracts this information from the observation information of consecutive time steps (by memorizing through the recursive loop) and thus transmits it to the RL system.

Finally, we use a ground truth baseline, which is a state directly extracted from the environment dynamics (see Section 4.2 for details in each environment), and an open-loop baseline, where the state is defined as the time step of an agent. The ground truth baseline is expected to constitute an upper bound on RL performance. The open-loop baseline serves as a sanity check. Indeed, the performance of SAC with this baseline on the three tasks allows us to validate whether these tasks really require closed-loop policy optimization. That is, whether it is necessary to use the agent’s perception and proprioceptive information to solve the task, or whether open-loop policy learning strategies may be sufficient. In particular, this gives the minimum performance to beat to show the relevance of different state representation strategies.

We justify the absence of state-of-the-art end-to-end RL baselines such as [Lee et al., 2019; Kostrikov et al., 2020; Laskin et al., 2020; Srinivas et al., 2020], despite their open source implementations, by their too high computational complexity which is impractical in our hardware setting and limited computational time.

## 4.2 Environment Details

We perform our experiments on the three environments presented in Fig. 3 which are all partially observable due to image observations. InvertedPendulum and HalfCheetah belong to the MuJoCo torque-controlled benchmark [Todorov et al., 2012], implemented on PyBullet [Coumans and Bai, 2019] (an open source library unlike MuJoCo). However, the MuJoCo benchmark was initially used from compact states directly provided by the simulator [Todorov et al., 2012]. In particular, while InvertedPendulum is easiest to control with a single torque, HalfCheetah, with its six torques, requires a state-of-the-art RL algorithm to solve its locomotion task even with compact states [Lillicrap et al., 2015].

We use the same number of action repetition as most works [Hafner et al., 2018; Yarats et al., 2019] (see Table 1). In many RL applications, the action is repeated several times to reduce the task horizon and make the control dynamics more stable. When the action is repeated, the number of observed time steps is reduced. For example with an action repetition of four, an episode of 1,000 total time steps is reduced to 250 observed time steps.

### 4.2.1 TurtleBot Maze

We have implemented this environment as a U-shaped maze with the TurtleBot robot from PyBullet [Coumans and Bai, 2019], inspired by Ant Maze from OpenAI Gym [Brockman et al., 2016] used by Shyam et al. [2019]. The two-dimensional action applies a velocity to each of the left and right wheels of the robot. The three-dimensional ground truth state is formed by the cartesian coordinates in x and y axis of the robot, and the angle of his orientation. In this environment, the task consists in a goal reaching task with sparse rewards and a long horizon<sup>2</sup>. Thus, it is a challenge for a RL algorithm to address the exploration/exploitation tradeoff. Specifically, this task provides a RL algorithm with

<sup>2</sup>In TurtleBot Maze, an agent must perform 47 actions of maximum amplitude to cross the maze.

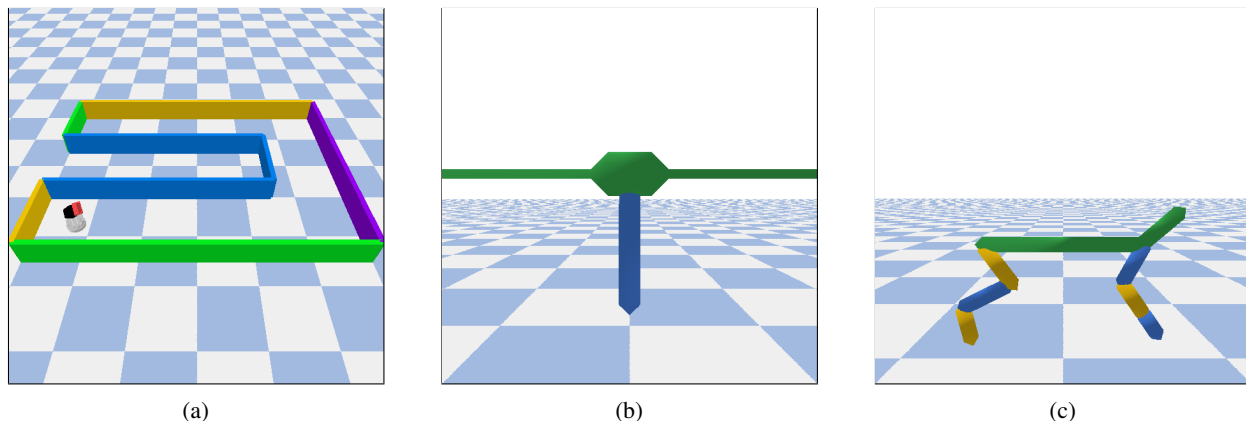


Figure 3: High-rendered images of the three continuous control environments in PyBullet [Coumans and Bai, 2019]. (a) The novel TurtleBot Maze environment proposed in this work, where the observation space corresponds to a first-person perspective camera, used to quantify XSRL exploration performance, and to provide a goal reaching task with navigation. (b) The InvertedPendulum environment provides a swing up task. (c) The HalfCheetah environment provides a locomotion task. (b), (c) are two popular torque-controlled benchmark environments where the observation space corresponds to the camera tracking an agent, as in the DMControl benchmark [Tassa et al., 2018].

a sparse reward of +1 each time the robot reaches the goal, a reward of -1 each time he touches a wall, and 0 otherwise, within a maximum of 100 time steps before the robot and the goal are randomly reinitialized. In addition, this task provides a RL algorithm with the position of the goal, which is concatenated to the state representation. Indeed, since the goal position is task-dependent, it cannot be learned by state representations in a rewardless SRL context.

#### 4.2.2 InvertedPendulum

The InvertedPendulum is attached to a pivot point on a cart sliding on a ramp. The one-dimensional action applies a force to the cart, which is limited to linear movement on the ramp. The five-dimensional ground truth state is formed by the x-axis position and velocity of the cart, the angular position in Cartesian space (i.e. cosine and sine of the angle) and angular velocity of the pendulum. In this environment, the task consists in a swing up task where the pendulum must swing up several times before balancing upward. Specifically, this task provides a RL algorithm with a reward for keeping the pendulum up vertically, within a maximum of 1,000 time steps before the pendulum is reset to a random state.

#### 4.2.3 HalfCheetah

The HalfCheetah is composed of eight rigid links, the torso and the back, and two legs each composed of three rigid and controllable links. The six-dimensional action applies torques to each of the six joints of the two legs. The 17-dimensional ground truth state is formed by the angular positions and velocities of the six joints, as well as agent cartesian position. In this environment, the task consists in a locomotion task where an agent must run to progress as far as possible. Specifically, this task provides a RL algorithm with a reward for moving the robot as fast as possible, in a maximum of 1,000 time steps and with a constraint that resets it to a random state as soon as it gets too close to the ground (which is not applied during XSRL and RAE trainings).

#### 4.2.4 Rewardless Environments

We detail some of the differences in the three environments used without reward in the SRL context and the three tasks described above used in the RL context. In the SRL context (i.e. during XSRL and RAE pretraining), an agent is reset after a longer horizon, and is initialized to a fixed state. For the TurtleBot Maze the horizon is 500 time steps, hence the need of an effective exploration to reach the other end of the maze, which is at the opposite of the fixed initial state. For the other two torque-controlled environments (InvertedPendulum and HalfCheetah), the horizon is 2,000 time steps (so 500 after repeating the action four times). The remaining common hyperparameters of the three environments for the SRL and RL contexts are displayed in Table 1.

#### 4.2.5 Image Preprocessing

The image preprocessing performed in these environments follows basically the same state-of-the-art approaches. Specifically, we divide the camera images by 255 to normalize them to  $[0, 1]$ . Then we downscale the image size to  $3 \times 64 \times 64$  pixels just like [Lillicrap et al., 2015; Sekar et al., 2020]. When the action repeat is one, an observation corresponds to the image  $\mathbf{o}_t = \mathbf{I}_t$ . When it is four, an observation corresponds to the stack of the three consecutive images  $\mathbf{o}_t = [\mathbf{I}_{t'-2}, \mathbf{I}_{t'-1}, \mathbf{I}_{t'}]$  of size  $9 \times 64 \times 64$ , just like [Lillicrap et al., 2015; Yarats et al., 2019], where  $t'$  corresponds to a time scale four times smaller than that of  $t$  (i.e.  $t' = 4 \times t$ ). For our XSRL method, this concatenation of images obtained by repeating the last action three times allows not to lose all the information on these time steps. Moreover, the estimation of the state at each time step where the action is repeated is far too computationally intensive to be feasible. Thus, this concatenation of images solves the trade-off between computational complexity and information loss. In practice for XSRL,  $\varphi$  uses  $\mathbf{o}_t$  to predict  $\mathbf{s}_{t+1}$ , from which  $\omega$  predicts the next observation  $\hat{\mathbf{o}}_{t+1}$ . In practice, RAE encodes  $\mathbf{o}_t$  into  $\mathbf{s}_t$  and decodes it into  $\hat{\mathbf{o}}_t$ .

#### 4.2.6 Test Datasets

For quantitative performance evaluation of our XSRL algorithm, we use an error measure of the next observation prediction, and for the state-of-the-art RAE baseline, we use an error measure of the next observation reconstruction. To perform those evaluations, we need an appropriate test dataset for each of the three environments described above. To do this, we carefully collected a wide variety of 400 transitions formed of observation-action pairs into a dataset. We generated them in two different ways. In the case of TurtleBot maze, we hand-designed expert trajectories that follow the U-shape of the maze. In the case of InvertedPendulum and HalfCheetah, we executed a policy learned by SAC from the ground truth baseline.

### 4.3 Implementation Details

We now detail the implementation of the training procedures for XSRL and SAC. Our implementation uses the deep learning library PyTorch [Paszke et al., 2017]. The hyperparameter details for XSRL are displayed in Table 3, and for SAC, when different from the original implementation of Haarnoja et al. [2018] in Table 2. Preliminary experiments showed that the hyperparameters  $w_{\mathcal{I}}$  and  $w_{\text{LPB}}$  (to solve the tradeoff during discovery policy training between maximizing the prediction error of an inverse model and maximizing the  $k$ -step learning progress bonus of  $\varphi$ ) had little impact on final performance.

For a fair comparison with RAE baseline, the same architecture as  $\alpha$  (a convolutional neural network) and  $\omega$  (a transposed convolutional neural network) is used for the encoder and decoder respectively. Similarly, for the random network baseline, the same architecture as  $\alpha$  is used to produce state representations but its randomly initialized parameters remain fixed. We choose as state dimensions for the TurtleBot Maze and InvertedPendulum environments 20 and for HalfCheetah 30 which correspond to heuristically chosen values, i.e. not very large but leading to good RL results.

We use the same architecture for the policy (a.k.a. actor model) and the action-value function (a.k.a. critic model) of the SAC algorithm as for the discovery policies, the inverse model and  $\gamma$  of our XSRL algorithm. As detailed in Table 3, our three-hidden layer architecture is different from the two-hidden layer architecture typically used in these same environments with image observations [Yarats et al., 2019; Hansen et al., 2020]. This deeper network architecture allows us to reduce the total number of parameters and thus the computational complexity. As Yarats et al. [2019], we use double Q-learning [Van Hasselt et al., 2015] for the critic model.

The Leaky Rectified Linear Unit (Leaky ReLU) is used for the activation functions between hidden layers, which removes the vanishing gradients encountered with the ReLU and improves the convergence speed and stability (which we observed empirically on preliminary experiments); see [Xu et al., 2015] for details.

In our RL experiments, the SAC algorithm is only used to test the generalization of the XSRL state representation to unseen control tasks. This implies that we keep the parameters of  $\varphi$  fixed. Due to memory constraints, for all experiments, we use a reduced buffer capacity unlike work comparable to ours: 100,000 instead of 1,000,000 with [Yarats et al., 2019].

#### 4.3.1 Hardware Details

All our experiments are performed on three computers, each containing 40 cores and a Titan xp GPU provided by Nvidia.

Table 1: Hyperparameters used in the PyBullet environments [Coumans and Bai, 2019].

Hyperparameter	Value
Image rendering size	$3 \times 96 \times 96$
Image size after downscaling	$3 \times 64 \times 64$
Action repeat	1 TurtleBot Maze 4 otherwise

Table 2: Hyperparameters used for SAC (Soft Actor-Critic [Haarnoja et al., 2018]) experiments.

Hyperparameter	Value
Episode length of the environments	100 TurtleBot Maze 1,000 otherwise
Discount factor $\gamma$	0.99
Replay buffer capacity	100,000
Optimizer	Adam [Kingma and Ba, 2014]
Batch size	256
Critic target update frequency	2
Actor update frequency	2
Learning rate for the critic model	$5e-4$
Learning rate for the actor model	$5e-4$
Learning rate for the automatic temperature tuning	$5e-4$
Entropy target $\bar{\mathcal{H}}$	$-\mathcal{A}_d$
Hidden units of critic/actor models	128, 512, 128



Table 3: Hyperparameters used for XSRL experiments.

Hyperparameter	Value
Episode length for all the environments (after action repeat)	500
State dimension $\mathcal{S}_d$	20 TurtleBot Maze; InvertedPendulum 30 HalfCheetah
$\alpha$ output dimension	30
$\beta$ output dimension	$(\mathcal{S}_d + \mathcal{A}_d)$
Intrinsic reward weight terms	$w_{\mathcal{I}} = 0.5, w_{\text{LPB}} = 1$
Optimizer	Adam [Kingma and Ba, 2014]
Batch size $B$ for $\alpha, \beta, \gamma, \omega$	32
Batch size $B_{\pi}$ for $\mathcal{I}$ and $\pi$	128
Update interval $T_{\pi}$ for $\mathcal{I}$ and $\pi$	512
Reset interval $T_{\text{reset}}$	4,096 for both discovery policies
Learning rate for $\alpha, \beta, \gamma, \omega$	1e-4
Learning rate for $\mathcal{I}$ and $\pi$	1e-4
Learning rate for $w_{\mathcal{H}}$	1e-4
Entropy target $\bar{\mathcal{H}}$	$-\mathcal{A}_d$
Hidden units of $\mathcal{I}, \pi, \gamma$	128, 512, 128
Hidden units of $\beta$	128, 512, 32
Hidden units of $\alpha, \omega$ :	
$\alpha$	CNN (strides and filters): (2, 32), (2, 64), (2, 128), (2, 256) MLP hidden units: 1024, 256, 32
$\omega$	MLP hidden units: 32, 256, 1024 transposed CNN (strides and filters): (1, 256), (2, 128), (2, 64), (2, 32)

## 5 Experimental Results

### 5.1 Evaluations of XSRL Representations and Exploration

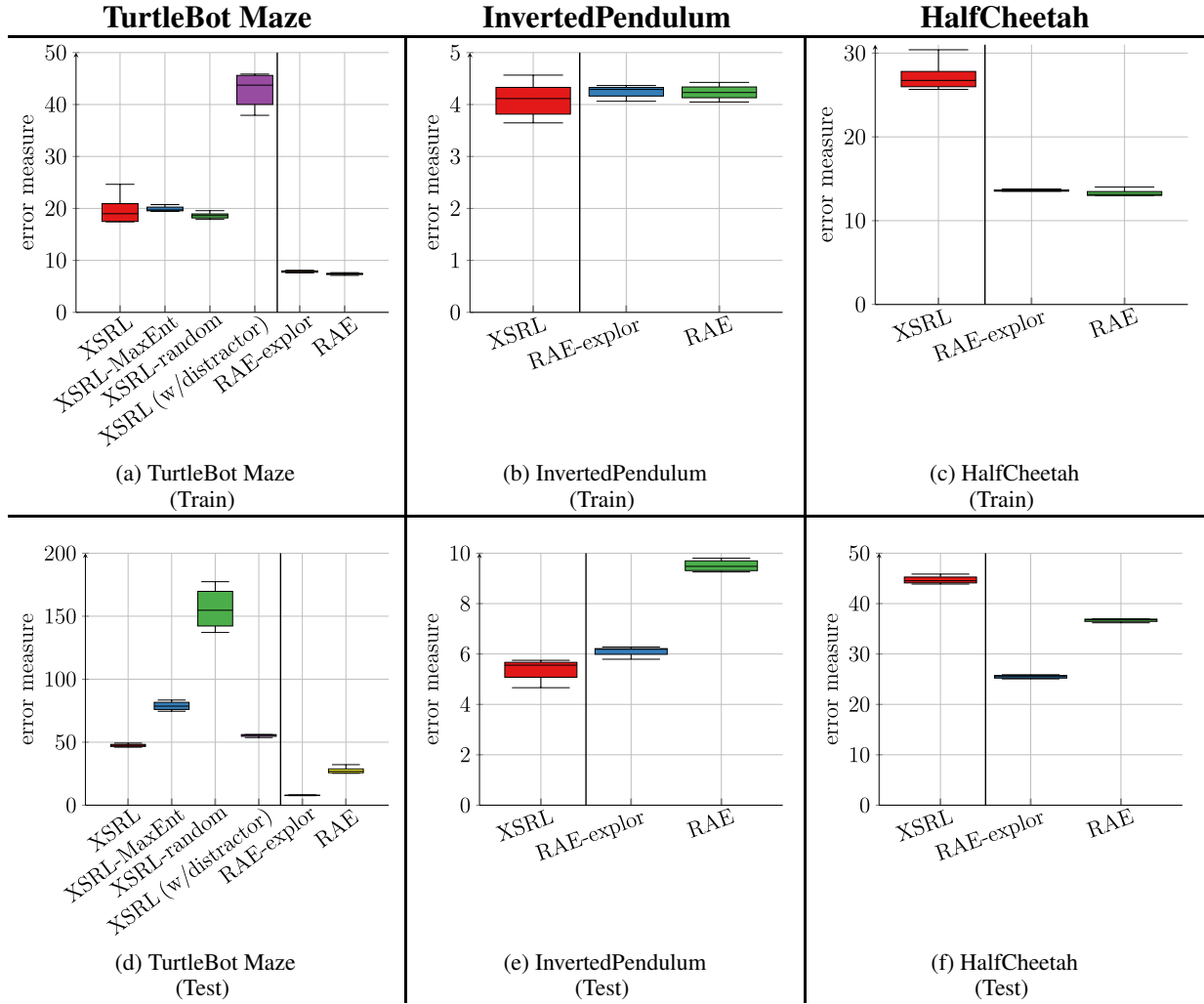


Figure 4: Error measure results (the lower the better) obtained on a training dataset (top row) and a test dataset (bottom row) (which is defined for each environment in Section 4.2.6), averaged over last 20 epochs across 5 runs (with a random seed). This measure corresponds to the prediction of  $\mathbf{o}_{t+1}$  with XSRL, and to the reconstruction of  $\mathbf{o}_{t+1}$  with RAE. XSRL (w/ distractor) is performed in TurtleBot Maze with a randomly sampled wall color.

In this section, we show the results of our quantitative and qualitative evaluations to validate whether XSRL verify criteria (i), (ii), and (iii) which we defined in Section 4.

Fig. 4 reports the results of the error measure obtained on a training dataset and a test dataset (defined in Section 4.2.6) on each of the three environments. This error measure corresponds to the prediction error of the next observation for XSRL and the two ablations (XSRL-random and XSRL-MaxEnt); it corresponds to the reconstruction error of the next observation for RAE [Ghosh et al., 2019] (following a random exploration) and RAE-explor (following an effective exploration, as explained in Section 4.1). We observe on the two environments, TurtleBot Maze and HalfCheetah, that the error measure for XSRL is higher than that for RAE and RAE-explor on both training and test datasets. This does not correspond to a poor exploration performance of XSRL but to the objective function which is more complicated than RAE. Indeed, all information in the next observation that cannot be predicted from the current time step is ignored as it is the case for random distractors or too complex information from the transition model, which tends to increase the prediction error. Furthermore, the qualitative results in Fig. 5 show that XSRL is able to predict very well what is

relevant to predict the next observation, but ignores less useful/redundant information. For example, in TurtleBot Maze it predicts the walls very well, but not the exact checkerboard pattern on the floor (see Fig. 5(i)).

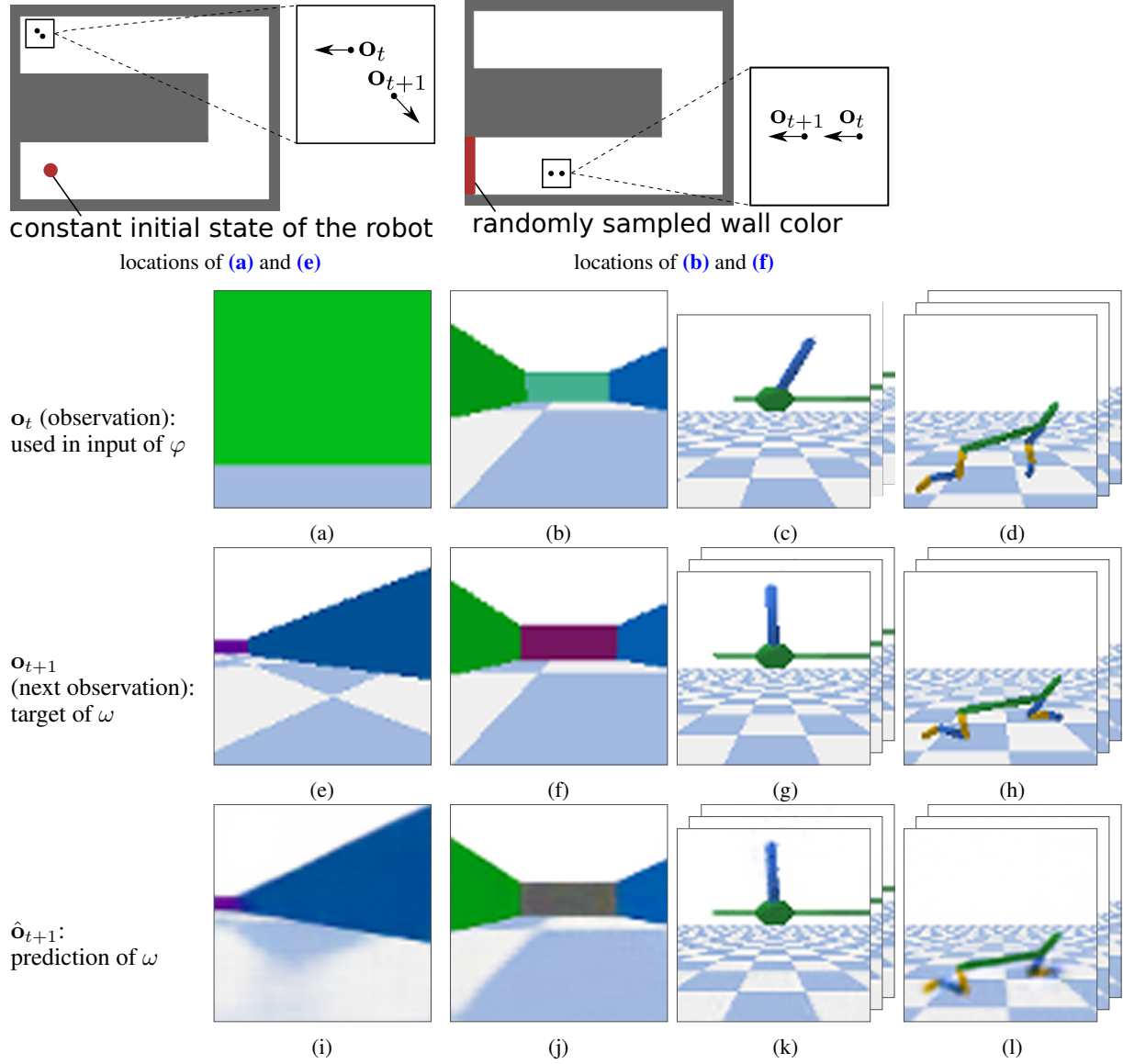


Figure 5: One of the most complex transitions in each of the test datasets (defined in Section 4.2.6) of environment from left to right: TurtleBot Maze, TurtleBot Maze w/ distractor, InvertedPendulum and HalfCheetah. The top line shows: (left) the locations of (a) and (e); (right) the locations of (b) and (f). In the bottom line, (i)-(l) show the corresponding  $\mathbf{o}_{t+1}$  predictions with XSRL. In (j) XSRL ignores the random wall color because it predicts a neutral gray color instead. For InvertedPendulum and HalfCheetah environments, as the action is repeated four times,  $\mathbf{o}_t$  corresponds to the three consecutive images  $[\mathbf{I}_{t'-2}, \mathbf{I}_{t'-1}, \mathbf{I}_{t'}]$  (as explained in Section 4.2.5).

These results therefore imply that representations learned by XSRL guarantee Markovian transitions which is criterion (i). In other words, the representations learned by XSRL succeed in retrieving information that allows the prediction of the next observation from the current time step. First, on the InvertedPendulum and HalfCheetah environments, since they are torque-controlled robots, the learned representations must retrieve the angular positions and velocities (which requires that the state representations memorize the information of the previous time step through the recursive loop) of their joints so that  $\omega$  can predict next observations. Second, on the TurtleBot Maze environment, the observation space is a first-person perspective camera, which constitutes a particularly complex partial observability setting. This complexity is amplified because the walls of the maze, as shown in Fig. 3(a) have only three colors for a total of eight walls. Therefore, when an agent is facing one of them, he cannot know his exact configuration (i.e. his position and



Figure 6: Visualization of the TurtleBot Maze exploration, where the color spectrum of the robot's position goes from purple (start of the episode) to yellow (end of the episode). The results obtained in the regular TurtleBot Maze environment correspond to: (a)-(e) XSRL, (f)-(j) XSRL-MaxEnt, (k)-(o) XSRL-random. The results obtained in TurtleBot Maze with a randomly sampled wall color correspond to: (p)-(t) XSRL, (u)-(y) XSRL-MaxEnt.

orientation) or even which wall it is. This phenomenon is known as perceptual aliasing [Cadena et al., 2016]. Thus, for XSRL representations to allow  $\omega$  to predict next observations, they must contain the robot's current configuration, which is only possible if they also verify the consistency and topology of the environment. The latter can be possible thanks to the recursive loop on state representations, which allows to memorize the information from the previous time steps (as explained in Section 3.1).

In TurtleBot Maze with a distractor represented by a randomly sampled wall color, the gray wall predicted by  $\omega$  in Fig. 5(j) shows that this random color is ignored by  $\varphi$ . This confirms that XSRL learns state representations which filter out stochastic information and more generally unnecessary information from observations, which is the criterion (ii).

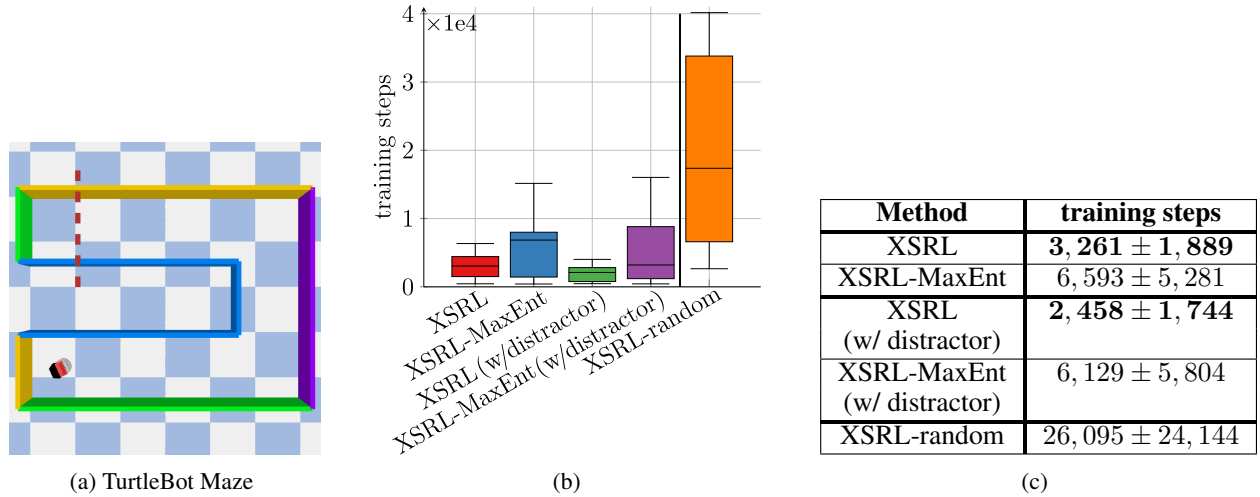


Figure 7: (a) Shows the top view of the TurtleBot Maze where the robot’s position corresponds to the constant initial state. (b), (c) Number of training steps before an agent crosses the dotted red line during XSRL training (mean  $\pm$  standard deviation over 10 runs; the lower the better). Our XSRL exploration strategy outperforms XSRL-MaxEnt, while XSRL-random provides an upper bound.

This also explains that the higher error measure results for XSRL are only related to unexploitable information with respect to its prediction objective.

We evaluated XSRL discovery policies through a comparative visualization of maze coverage displayed in Fig. 6, accompanied by a quantitative evaluation of maze exploration presented in Fig. 7. We observe in Fig. 6 that on a trajectory of 1,000 time steps, XSRL exploration reaches the farthest transitions much faster than XSRL-MaxEnt, while XSRL-random almost never does. Moreover, the trajectories generated by XSRL and XSRL-MaxEnt policies shown in Fig. 6 are not attracted to transitions with the distractor related to randomly sampled wall color near which the agent is initialized.

Fig. 7 shows that XSRL policies accelerate the probability that agents reach the other end of the maze in 500 time steps during pretraining. Specifically, with XSRL-random, agents can almost never reach the other end of the maze in only 500 time steps. Unlike the previous one, the exploration with XSRL and XSRL-MaxEnt use the visited state as input, which could lead an agent to always prefer transitions with a distractor (as analyzed by Burda et al. [2018]). However, we observe no difference in performance with a distractor in TurtleBot Maze, which also confirms criterion (ii). Moreover, with and without a distractor, XSRL exploration reaches the end of the maze almost twice as fast as with XSRL-MaxEnt. These results thus confirm that XSRL discovery policies are successful in guiding agents quickly to diverse and learnable transitions, which is criterion (iii).

Given the previous qualitative and quantitative results, we interpret the performances of the exploration with XSRL and XSRL-MaxEnt as follows: XSRL discovery policies allow to visit the farthest transitions quickly because they tend to produce larger  $k$ -step learning progress bonuses of  $\varphi$ . They also visit more transitions that cause directional changes because they tend to produce larger prediction errors of a trained inverse model. On the contrary, XSRL-MaxEnt policies follow various paths without preferring the transitions farthest from the constant initial state (i.e. to the other end of the maze), even though the prediction errors of the next observation on these transitions are larger.

The video available here <https://youtu.be/IbGa-TC7wek>, shows a comparative evaluation between XSRL exploration (left) and random exploration (right) in each of the three environments. It highlights that discovery policies learned by XSRL allow: in TurtleBot Maze to quickly visit transitions far from the initial state position (as shown in the previous results); in InvertedPendulum to move the pendulum upwards while it is initialized downwards with zero velocity; in HalfCheetah to keep the robot constantly moving. We can see that for random exploration: in TurtleBot Maze the robot moves little away from its initial state; in InvertedPendulum the pendulum is never upwards; in HalfCheetah it is complicated for the robot to stay constantly in motion since it ends up stuck in a lying position.

In addition to these qualitative and quantitative comparisons, the better performance of XSRL exploration is also confirmed by the quantitative evaluation of the prediction error measure displayed in Fig. 4. This measure reaches its lowest value with XSRL exploration, followed by XSRL-MaxEnt and finally XSRL-random which is by far the worst strategy.



Apart from the comparative study of our XSRL exploration, we observe that an effective exploration improves the generalization performance of RAE models. Indeed, the quantitative evaluation of the observation reconstruction (see Fig. 4) shows a smaller error on the test dataset with RAE-explor (which is trained with an efficient exploration as explained in Section 4.1) than with RAE. Thus, training on diverse transitions improves the generalization performance of observation reconstruction with RAE.

Qualitative and quantitative performance differences with respect to exploration strategies show the advantage of visiting quickly diverse transitions during state embedding pretraining to obtain better generalization performance over new transitions. However, as we see below, it is only with the XSRL prediction error measure that this generalization performance is sure to translate into good transfer performance with a new RL task.

## 5.2 XSRL Representations Transfer

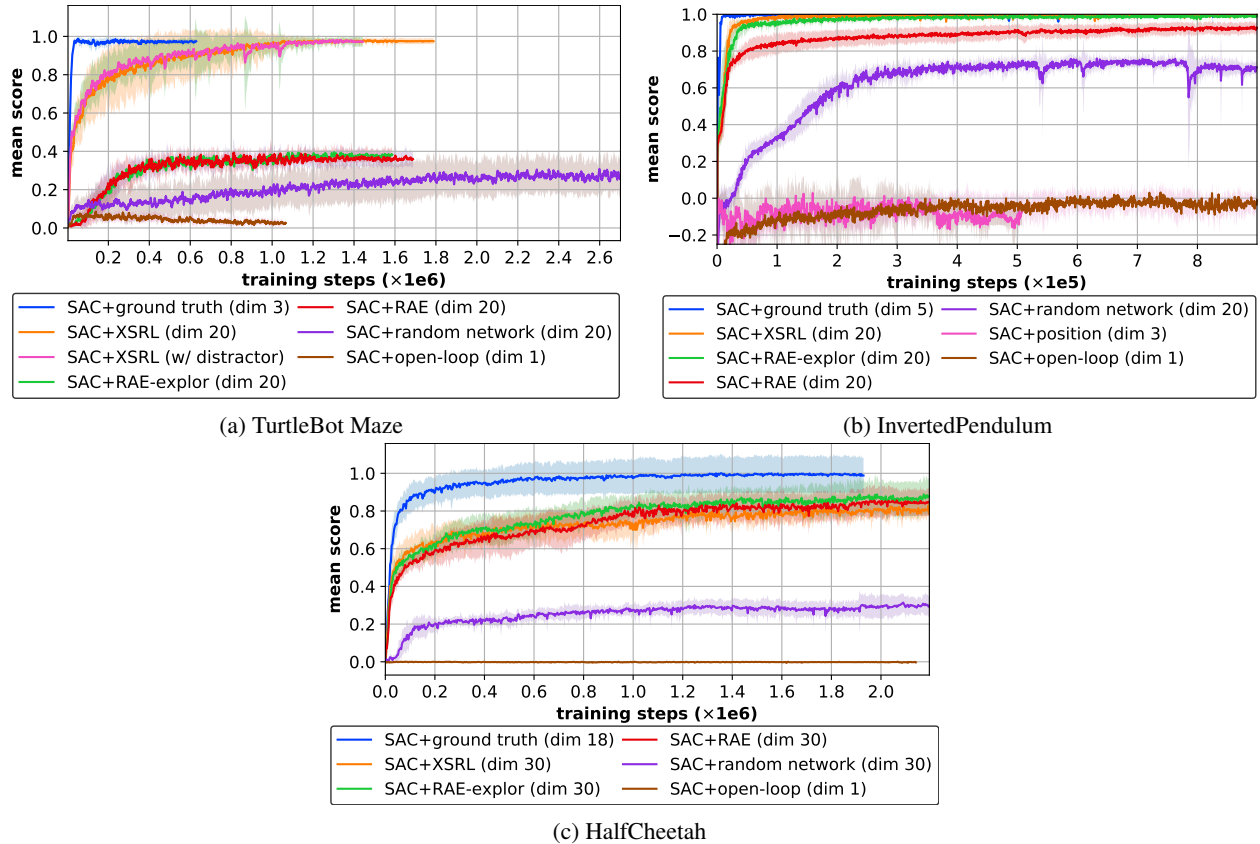


Figure 8: Learning curves of the episode returns averaged over 10 episodes (mean in lines and standard deviation in shaded areas over 10 runs; the higher the better) of SAC with different state representation strategies on three different continuous control tasks. The XSRL pretrained representations are the only one to perform well in three of the environments, while ground truth and open-loop provide an upper and lower bound respectively. A video showing the corresponding optimal policies can be found at <https://youtu.be/XpRcU75i-iQ>.

In this section, we show quantitative evaluations to validate whether state estimators pretrained with our algorithm (XSRL) provide advantageous inputs to RL systems for solving three unseen control tasks (which is an instance of criterion (iv) defined in Section 4). In particular, we use the deep RL algorithm SAC (Soft Actor-Critic) [Haarnoja et al., 2018] which has shown promising results on the standard continuous control tasks InvertedPendulum and HalfCheetah. Throughout these experiments, all parameters of the pretrained state embeddings (with XSRL and RAE) are kept fixed: only the actor and critic neural networks of SAC are trained. We performed 10 runs with a random seed just like [Henderson et al., 2018; Yarats et al., 2019], resulting in 10 different trained policies for each of the representation strategies. For each state embedding pretraining approach (XSRL and RAE) and for the random network, we used 5 different models trained with a random seed, from which 2 SAC runs with a random seed are executed. In

Table 4: Episode returns after convergence of the curves in Fig. 8 averaged over 100 episodes (mean  $\pm$  standard deviation over 10 runs; the higher the better).

Mean score	TurtleBot Maze	InvertedPendulum	HalfCheetah
SAC+XSRL	<b><math>0.98 \pm 0.02</math></b>	<b><math>1 \pm 0</math></b>	$0.82 \pm 0.03$
SAC+RAE-explor	$0.34 \pm 0.04$	$0.99 \pm 0$	<b><math>0.87 \pm 0.09</math></b>
SAC+RAE	$0.34 \pm 0.06$	$0.93 \pm 0.03$	$0.85 \pm 0.08$
SAC+random network	$0.27 \pm 0.1$	$0.74 \pm 0.02$	$0.31 \pm 0.05$
SAC+ground truth	$0.98 \pm 0.02$	$1 \pm 0$	$1 \pm 0.1$
SAC+open-loop	$0.04 \pm 0.03$	$0 \pm 0.06$	$0 \pm 0$

addition, unlike ground truth, open-loop and position baselines, they transform visual observations into compact state representations of 20 dimensions for TurtleBot Maze and InvertedPendulum, and 30 dimensions<sup>3</sup> for HalfCheetah.

Fig. 8 shows the learning curves of the episode returns averaged over 10 episodes across 10 runs. After training, we measured the episode returns averaged over 100 episodes for the 10 trained policies, which are displayed in Table 4. For clarity, we normalized all episode returns between the average SAC+ground truth performance and that of SAC+open-loop, except for the task with TurtleBot Maze as this is evaluated with the probability to reach the goal (from a random initial configuration) in 100 time steps or less. Indeed, SAC+ground truth is an upper bound because it has easy access to the agent’s proprioceptive information, and SAC+open-loop is a lower bound because it corresponds to a blind agent. These results show that only XSRL state representations perform well in all three RL problems, unlike the other state representation baselines.

Fig. 8(b) shows that the position baseline does not allow SAC to learn a good policy on the InvertedPendulum task. This confirms that InvertedPendulum and HalfCheetah tasks require information from the positions and velocities of the agent’s joints to verify Markovian state transitions which are only related to the local consistency of the environment. On InvertedPendulum, SAC+XSRL and SAC+RAE-explor reach same performance as SAC+ground truth, SAC+RAE follows right after, and even lower follows SAC+random network which reaches a mean score of 0.74. On HalfCheetah, we obtain in decreasing order of performance: SAC+RAE-explor, SAC+RAE, SAC+XSRL, SAC+random network. While the first three performances are similar with a score of about 0.85, SAC+random network is well below with about 0.3.

In TurtleBot Maze, none of the state representation strategies other than XSRL were successful on the navigation task. Specifically, SAC+XSRL reaches the same performance as SAC+ground truth; SAC+RAE-explor and SAC+RAE reach the same score of 0.34, while SAC+random network is just below with a score of 0.27 but has much slower convergence. This shows that only the XSRL representations verify the local consistency and topology of the environment to retrieve the orientation and position of an agent. As explained earlier in Section 3, these properties of the representations are required to make state transitions Markovian due to perceptual aliasing [Cadena et al., 2016]. Furthermore, as shown by Fig. 8(a), the performance of SAC+XSRL is the same in TurtleBot Maze with a distractor. This confirms that by memorizing the information useful for predicting the next observation and filtering out all the other information, the XSRL representations contain the information in a way that can control the robot.

According to these results, it is more difficult to learn state embeddings that encode the environment properties independent of an agent (i.e. topology) than those that depend on him (i.e. local consistency). Overall, these quantitative evaluations show that pretrained state estimators with XSRL provide advantageous inputs to solve unseen control tasks with SAC algorithm, which is an instance of criterion (iv).

## 6 Discussion

Experimental results show that the proposed XSRL algorithm builds state representations that are the only ones to perform well on the three unseen RL tasks. We see the link between the generalization performance of XSRL with respect to the next observation prediction (see Table 4) and the transfer performance of its pretrained state estimator ( $\varphi$ ) to a new RL system (see Table 4). More specifically, the good prediction performance on a test dataset of state embeddings pretrained with XSRL guarantees their good transfer performance to new RL tasks.

As we have seen, the generalization performance on the test dataset strongly depends on the exploration efficiency (see Fig. 4), which is better with XSRL than with its two ablations. Moreover, our exploration allows agents to reach

<sup>3</sup>The numbers of 20 and 30 dimensions were empirically selected to account for the trade-off between sample efficiency and final performance (i.e. between computation time and the optimal policy performance).

transitions far away from their initial states and much faster than the policy entropy maximization and random strategies (see Fig. 7). Hence the link between fast exploration of various transitions and good generalization.

However, the strategy of maximizing the policy entropy works well for learning policies with extrinsic rewards in the RL context. In particular, Eysenbach and Levine [2021] show in a navigation task with obstacles that it allows to increase the exploration diversity of an agent and thus to more efficiently bypass obstacles than with a random exploration where he would remain blocked.

In contrast to XSRL, our results showed that the good reconstruction performance of state embeddings pretrained with RAE did not always guarantee good transfer to RL tasks. Specifically, no matter how much RAE models minimize the reconstruction error on the test dataset of TurtleBot Maze, RL systems will perform poorly with inputs from this type of representation.

Finally, we analyze the results of SAC+XSRL across the three different continuous control tasks. While in TurtleBot Maze and InvertedPendulum SAC+XSRL obtains performances equal to those of SAC+ground truth, in HalfCheetah its performance is lower (0.82) and close to SAC+RAE (0.85). Moreover, this poorer performance is accompanied by a failure during the pretrainings of XSRL models, since they obtain abnormally high prediction errors on the training datasets. Indeed, comparing this prediction performance on the most similar environment InvertedPendulum (because it does not present perceptual aliasing) we have in Table 4: 4.2 on InvertedPendulum, 27.6 on HalfCheetah. Furthermore, as we have already discussed, XSRL exploration allows in HalfCheetah to keep the robot in constant motion, whereas random exploration cannot because the robot quickly gets stuck in a lying position<sup>4</sup>. Therefore, the lower performance of SAC+XSRL in the HalfCheetah task is likely due to poor modeling of the transition model, as the result of the next observation prediction in Fig. 5(l) tends to confirm. Indeed, it shows that there are errors in the next observation prediction related to the positions of the robot joints, which proves that the state transition estimator has not been well modeled. This could be explained by the high complexity of the transitions generated by HalfCheetah using a torque control. Moreover, due to the high number of degrees of freedom (six), the properties of its dynamics are much more unstable than those of InvertedPendulum (only two degrees of freedom), and far more than those of TurtleBot Maze, the latter using a velocity control.

While there are sources of prediction errors that  $\varphi$  fails to reduce,  $\varphi$  forces compact state representations to discard information related to aleatoric uncertainty (as we explained in Section 3.1). Achieving robustness to random distractors is a common goal of the state estimation techniques initiated by Kalman [1960]. However, some random distractors can sometimes be useful in specific control tasks. For example, in a task where an agent must follow a behavior only when a lamp that randomly changes color is green. Since this information is random, it will be unpredictable to XSRL and thus filtered by its state representations. To deploy the state transition estimator to this specific task, it is therefore necessary to concatenate to output of  $\varphi$  a vector representing the color of the lamp (either handcrafted or learned) so that a RL algorithm can properly exploit this information.

Overall, experimental results have highlighted the main advantage of XSRL in learning state embeddings which are able to verify both the local consistency of the environment and its topology. While the state-of-the-art RAE method succeeds perfectly in encoding the former, it fails completely in encoding the latter, as shown by the RL results with the TurtleBot Maze task (see Table 4). By evaluating XSRL with one transfer scenario where it outperforms a state-of-the-art method, and with another scenario where XSRL comes on par with it, we follow the experimental recommendations of Henderson et al. [2018] to prove that our new XSRL method matters for RL transfer scenarios.

## 7 Conclusion

We have presented a SRL algorithm (XSRL) for pretraining state representations from next observation prediction errors by extending the understudied discovery faculty we realized with a new exploration strategy, that trains discovery policies to sample the most diverse and learnable unknown transitions. Our experiments show that XSRL exploration provides fast maze traversal compared to traditional random policy and policy entropy maximization strategies. Moreover, our comparative evaluation on unseen RL tasks confirmed the transfer efficiency of the pretrained XSRL models. One of the most striking results is the superiority of XSRL representations over autoencoder ones, which is obviously due to better representational properties since the underlying data manifold (i.e. agent and environment degrees of freedom) is constrained to follow Markovian transitions with respect to the prediction objective. Furthermore, these results illustrate the importance of the overlooked discovery faculty and suggest that an exploration strategy in the SRL framework can lead to better state representation pretraining approaches.

<sup>4</sup>See the video available at <https://youtu.be/IbGa-TC7wek>

## Author Contributions

AM: designed the proposed algorithm, implemented the experiments, and also wrote the article. SD,NPG, and AC: supervised the project and provided guidance and feedback, and also helped with the writing of the article.

## Funding

This work has been sponsored by the Labex SMART supported by French state funds managed by the ANR within the Investissements d’Avenir program under references ANR-11-LABX-65 and ANR-18-CE33-0005 HUSKI, and by the FET project VeriDream that has received funding from the European Union’s H2020-EU.1.2.2. research and innovation program under grant agreement No 951992. We gratefully acknowledge the support of NVIDIA Corporation with the donation of one Titan Xp GPU used for this research.

## References

- Achiam, J. and Sastry, S. (2017). Surprise-based intrinsic motivation for deep reinforcement learning. *arXiv preprint arXiv:1703.01732*.
- Assael, J.-A. M., Wahlström, N., Schön, T. B., and Deisenroth, M. P. (2015). Data-efficient learning of feedback policies from image pixels using deep dynamical models. *arXiv preprint arXiv:1510.02173*.
- Böhmer, W., Grünwälder, S., Shen, Y., Musial, M., and Obermayer, K. (2013). Construction of approximation spaces for reinforcement learning. *The Journal of Machine Learning Research*, 14(1):2067–2118.
- Böhmer, W., Springenberg, J. T., Boedecker, J., Riedmiller, M., and Obermayer, K. (2015). Autonomous learning of state representations for control: An emerging field aims to autonomously learn state representations for reinforcement learning agents from their real-world sensor observations. *KI-Künstliche Intelligenz*, 29(4):353–362.
- Brockman, G., Cheung, V., Pettersson, L., Schneider, J., Schulman, J., Tang, J., and Zaremba, W. (2016). Openai gym. *arXiv preprint arXiv:1606.01540*.
- Bubeck, S., Munos, R., and Stoltz, G. (2009). Pure exploration in multi-armed bandits problems. In *International conference on Algorithmic learning theory*, pages 23–37. Springer.
- Burda, Y., Edwards, H., Pathak, D., Storkey, A., Darrell, T., and Efros, A. A. (2018). Large-scale study of curiosity-driven learning. *arXiv preprint arXiv:1808.04355*.
- Cadena, C., Carlone, L., Carrillo, H., Latif, Y., Scaramuzza, D., Neira, J., Reid, I., and Leonard, J. J. (2016). Past, present, and future of simultaneous localization and mapping: Toward the robust-perception age. *IEEE Transactions on robotics*, 32(6):1309–1332.
- Coumans, E. and Bai, Y. (2016–2019). Pybullet, a python module for physics simulation for games, robotics and machine learning. <http://pybullet.org>.
- de Bruin, T., Kober, J., Tuyls, K., and Babuška, R. (2018). Integrating state representation learning into deep reinforcement learning. *IEEE Robotics and Automation Letters*, 3(3):1394–1401.
- Eysenbach, B. and Levine, S. (2021). Maximum entropy rl (provably) solves some robust rl problems. <https://arxiv.org/pdf/2103.06257.pdf>.
- Gaier, A. and Ha, D. (2019). Weight agnostic neural networks. In *Advances in Neural Information Processing Systems*, pages 5364–5378.
- Ghosh, P., Sajjadi, M. S., Vergari, A., Black, M., and Schölkopf, B. (2019). From variational to deterministic autoencoders. *arXiv preprint arXiv:1903.12436*.
- Glasmachers, T. (2017). Limits of end-to-end learning. In Zhang, M. and Noh, Y., editors, *Proceedings of The 9th Asian Conference on Machine Learning, ACML 2017, Seoul, Korea, November 15-17, 2017*, volume 77 of *Proceedings of Machine Learning Research*, pages 17–32. PMLR.
- Haarnoja, T., Zhou, A., Hartikainen, K., Tucker, G., Ha, S., Tan, J., Kumar, V., Zhu, H., Gupta, A., Abbeel, P., and Levine, S. (2018). Soft actor-critic algorithms and applications. *CoRR*, abs/1812.05905.
- Hafner, D., Lillicrap, T., Fischer, I., Villegas, R., Ha, D., Lee, H., and Davidson, J. (2018). Learning latent dynamics for planning from pixels. *arXiv preprint arXiv:1811.04551*.
- Hansen, N., Sun, Y., Abbeel, P., Efros, A. A., Pinto, L., and Wang, X. (2020). Self-supervised policy adaptation during deployment. *CoRR*, abs/2007.04309.

- Henderson, P., Islam, R., Bachman, P., Pineau, J., Precup, D., and Meger, D. (2018). Deep reinforcement learning that matters. In *Thirty-Second AAAI Conference on Artificial Intelligence*.
- Hester, T. and Stone, P. (2012). Intrinsically motivated model learning for a developing curious agent. In *2012 IEEE international conference on development and learning and epigenetic robotics (ICDL)*, pages 1–6. IEEE.
- Jaderberg, M., Mnih, V., Czarnecki, W. M., Schaul, T., Leibo, J. Z., Silver, D., and Kavukcuoglu, K. (2017). Reinforcement learning with unsupervised auxiliary tasks. In *5th International Conference on Learning Representations, ICLR 2017, Toulon, France, April 24-26, 2017, Conference Track Proceedings*. OpenReview.net.
- Jarrett, K., Kavukcuoglu, K., Ranzato, M., and LeCun, Y. (2009). What is the best multi-stage architecture for object recognition? In *2009 IEEE 12th international conference on computer vision*, pages 2146–2153. IEEE.
- Jonschkowski, R. and Brock, O. (2013). Learning task-specific state representations by maximizing slowness and predictability. In *6th international workshop on evolutionary and reinforcement learning for autonomous robot systems (ERLARS)*.
- Kalman, R. E. (1960). A new approach to linear filtering and prediction problems.
- Kingma, D. P. and Ba, J. (2014). Adam: A method for stochastic optimization. *arXiv preprint arXiv:1412.6980*.
- Kingma, D. P. and Welling, M. (2014). Auto-encoding variational bayes. In Bengio, Y. and LeCun, Y., editors, *2nd International Conference on Learning Representations, ICLR 2014, Banff, AB, Canada, April 14-16, 2014, Conference Track Proceedings*.
- Kostrikov, I., Yarats, D., and Fergus, R. (2020). Image augmentation is all you need: Regularizing deep reinforcement learning from pixels. *CoRR*, abs/2004.13649.
- Lange, S. and Riedmiller, M. (2010). Deep auto-encoder neural networks in reinforcement learning. In *The 2010 International Joint Conference on Neural Networks (IJCNN)*, pages 1–8. IEEE.
- Laskin, M., Lee, K., Stooke, A., Pinto, L., Abbeel, P., and Srinivas, A. (2020). Reinforcement learning with augmented data. *CoRR*, abs/2004.14990.
- Lee, A. X., Nagabandi, A., Abbeel, P., and Levine, S. (2019). Stochastic latent actor-critic: Deep reinforcement learning with a latent variable model. *arXiv preprint arXiv:1907.00953*.
- Lesort, T., Díaz-Rodríguez, N., Goudou, J.-F., and Filliat, D. (2018). State representation learning for control: An overview. *Neural Networks*, 108:379–392.
- Li, Y. (2018). Deep reinforcement learning. *CoRR*, abs/1810.06339.
- Lillicrap, T. P., Hunt, J. J., Pritzel, A., Heess, N., Erez, T., Tassa, Y., Silver, D., and Wierstra, D. (2015). Continuous control with deep reinforcement learning. *arXiv preprint arXiv:1509.02971*.
- Lopes, M., Lang, T., Toussaint, M., and Oudeyer, P.-Y. (2012). Exploration in model-based reinforcement learning by empirically estimating learning progress. In *Advances in neural information processing systems*, pages 206–214.
- Morik, M., Rastogi, D., Jonschkowski, R., and Brock, O. (2019). State representation learning with robotic priors for partially observable environments. In *IROS*, pages 6693–6699.
- Oudeyer, P.-Y., Kaplan, F., and Hafner, V. V. (2007). Intrinsic motivation systems for autonomous mental development. *IEEE transactions on evolutionary computation*, 11(2):265–286.
- Paszke, A., Gross, S., Chintala, S., Chanan, G., Yang, E., DeVito, Z., Lin, Z., Desmaison, A., Antiga, L., and Lerer, A. (2017). Automatic differentiation in pytorch.
- Pathak, D., Agrawal, P., Efros, A. A., and Darrell, T. (2017). Curiosity-driven exploration by self-supervised prediction. In *International Conference on Machine Learning (ICML)*, volume 2017.
- Pathak, D., Gandhi, D., and Gupta, A. (2019). Self-supervised exploration via disagreement. *arXiv preprint arXiv:1906.04161*.
- Sekar, R., Rybkin, O., Daniilidis, K., Abbeel, P., Hafner, D., and Pathak, D. (2020). Planning to explore via self-supervised world models. *arXiv preprint arXiv:2005.05960*.
- Shelhamer, E., Mahmoudieh, P., Argus, M., and Darrell, T. (2017). Loss is its own reward: Self-supervision for reinforcement learning. *arXiv preprint arXiv:1612.07307*.
- Shyam, P., Jaśkowski, W., and Gomez, F. (2019). Model-based active exploration. In *International Conference on Machine Learning*, pages 5779–5788. PMLR.
- Srinivas, A., Laskin, M., and Abbeel, P. (2020). Curl: Contrastive unsupervised representations for reinforcement learning. *CoRR*, abs/2004.04136.



- Tassa, Y., Doron, Y., Muldal, A., Erez, T., Li, Y., Casas, D. d. L., Budden, D., Abdolmaleki, A., Merel, J., Lefrancq, A., et al. (2018). Deepmind control suite. *arXiv preprint arXiv:1801.00690*.
- Todorov, E., Erez, T., and Tassa, Y. (2012). Mujoco: A physics engine for model-based control. In *Intelligent Robots and Systems (IROS), 2012 IEEE/RSJ International Conference on*, pages 5026–5033. IEEE.
- Van Hasselt, H., Guez, A., and Silver, D. (2015). Deep reinforcement learning with double q-learning. *arXiv preprint arXiv:1509.06461*.
- van Hoof, H., Chen, N., Karl, M., van der Smagt, P., and Peters, J. (2016). Stable reinforcement learning with autoencoders for tactile and visual data. In *Intelligent Robots and Systems (IROS), 2016 IEEE/RSJ International Conference on*, pages 3928–3934. IEEE.
- Wahlström, N., Schön, T. B., and Deisenroth, M. P. (2015). From pixels to torques: Policy learning with deep dynamical models. *arXiv preprint arXiv:1502.02251*.
- Watter, M., Springenberg, J., Boedecker, J., and Riedmiller, M. (2015). Embed to control: A locally linear latent dynamics model for control from raw images. In *Advances in neural information processing systems*, pages 2746–2754.
- Xu, B., Wang, N., Chen, T., and Li, M. (2015). Empirical evaluation of rectified activations in convolutional network. *arXiv preprint arXiv:1505.00853*.
- Yarats, D., Zhang, A., Kostrikov, I., Amos, B., Pineau, J., and Fergus, R. (2019). Improving sample efficiency in model-free reinforcement learning from images. *CoRR*, abs/1910.01741.